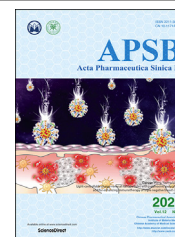




Chinese Pharmaceutical Association
Institute of Materia Medica, Chinese Academy of Medical Sciences

Acta Pharmaceutica Sinica B

www.elsevier.com/locate/apsb
www.sciencedirect.com



ORIGINAL ARTICLE

Discovery of novel KRAS–PDE δ inhibitors with potent activity in patient-derived human pancreatic tumor xenograft models



Long Chen^{a,†}, Jing Zhang^{b,†}, Xinjing Wang^{c,d,†}, Yu Li^a, Lu Zhou^e,
Xiongxiong Lu^{c,d,*}, Guoqiang Dong^{a,*}, Chunquan Sheng^{a,*}

^aSchool of Pharmacy, Second Military Medical University, Shanghai 200433, China

^bDepartment of Pathology, Changzheng Hospital, Second Military Medical University, Shanghai 200003, China

^cDepartment of General Surgery, Pancreatic Disease Center, Ruijin Hospital, Shanghai Jiao Tong University, Shanghai 200025, China

^dResearch Institute of Pancreatic Diseases, Shanghai Jiao Tong University School of Medicine, Shanghai 200025, China

^eDepartment of Medicinal Chemistry, School of Pharmacy, Fudan University, Shanghai 201203, China

Received 19 April 2021; received in revised form 3 July 2021; accepted 5 July 2021

KEY WORDS

KRAS–PDE δ interaction;
PDX;
Spiro-cyclic inhibitors;
Lead optimization;
SBDD;
Anti-pancreatic cancer
activity

Abstract KRAS–PDE δ interaction is revealed as a promising target for suppressing the function of mutant KRAS. The bottleneck in clinical development of PDE δ inhibitors is the poor antitumor activity of known chemotypes. Here, we identified novel spiro-cyclic PDE δ inhibitors with potent antitumor activity both *in vitro* and *in vivo*. In particular, compound **361** ($K_D = 127 \pm 16$ nmol/L) effectively bound to PDE δ and interfered with KRAS–PDE δ interaction. It influenced the distribution of KRAS in Mia PaCa-2 cells, downregulated the phosphorylation of t-ERK and t-AKT and promoted apoptosis of the cells. The novel inhibitor **361** exhibited significant *in vivo* antitumor potency in pancreatic cancer patient-derived xenograft (PDX) models. It represents a promising lead compound for investigating the druggability of KRAS–PDE δ interaction.

© 2022 Chinese Pharmaceutical Association and Institute of Materia Medica, Chinese Academy of Medical Sciences. Production and hosting by Elsevier B.V. This is an open access article under the CC BY-NC-ND license (<http://creativecommons.org/licenses/by-nc-nd/4.0/>).

*Corresponding authors. Tel./fax: +86 21 64370045 671003 (Xiongxiong Lu), +86 21 81871242 (Guoqiang Dong), +86 21 81871239 (Chunquan Sheng).

E-mail addresses: simone515night@126.com (Xiongxiong Lu), gdong@smmu.edu.cn (Guoqiang Dong), shengcq@hotmail.com, shengcq@smmu.edu.cn (Chunquan Sheng).

[†]These authors made equal contributions to this work.

Peer review under responsibility of Chinese Pharmaceutical Association and Institute of Materia Medica, Chinese Academy of Medical Sciences.

<https://doi.org/10.1016/j.apsb.2021.07.009>

2211-3835 © 2022 Chinese Pharmaceutical Association and Institute of Materia Medica, Chinese Academy of Medical Sciences. Production and hosting by Elsevier B.V. This is an open access article under the CC BY-NC-ND license (<http://creativecommons.org/licenses/by-nc-nd/4.0/>).

1. Introduction

Pancreatic cancer is one of the most fatal solid tumor with a high recurrence rate and poor prognosis^{1,2}. Mutations in KRAS gene are considered to be a key factor of pancreatic cancer progression^{3,4}. However, the development of KRAS-targeting antitumor agents is highly challenging and a number of drug candidates failed in clinical trials^{5,6}. Recently, the development of KRAS^{G12C} inhibitors has gained great attention^{7–9}, which shows promising results in phase I clinical trial^{10–12}. However, KRAS^{G12C} is a comparatively minority of the KRAS mutation spectrum (approximately 11%)¹³, inhibitors of other KRAS mutation subtypes, such as KRAS^{G12D} and KRAS^{G12V}, remain to be further investigated^{14,15}.

Chaperone protein PDE δ plays an essential role in the function of KRAS protein in the cells^{16–18}. PDE δ enhances the diffusion of KRAS in the cytoplasm by binding the farnesyl group, and promotes its distribution over intracellular membrane¹⁸. Down-modulation or inhibition of PDE δ protein suppresses KRAS signaling, and inhibits the growth and proliferation of cancer cells¹⁷.

KRAS–PDE δ interaction has been proposed as a potential target for the development of novel antitumor agents. Currently, a series of KRAS–PDE δ inhibitors have been reported (Fig. 1)¹⁹. Waldmann's group¹⁷ discovered the first KRAS–PDE δ inhibitor deltarasin (**1**) by fragment based drug design (FBDD) at 2013. However, the selectivity of deltarasin was poor, which showed apparent cytotoxicity²⁰. Subsequently, more selective inhibitors deltazinsonone (**2**) and deltasonamide (**3**) were designed^{20–22}. Although these inhibitors generally showed high PDE δ binding affinity, further development was hampered by poor cellular potency and metabolic stability. More recently, triazole inhibitor (**4**)²³, tetrahydrodibenzofuran inhibitor NHTD (**5**)²⁴ and coumarin inhibitor deltaflexin (**6**)²⁵ were reported. However, the antitumor efficacy of known PDE δ inhibitors remains to be significantly improved. Previously, our group reported the discovery and optimization of quinazolinone KRAS–PDE δ inhibitors **7** and **8** based on structural biology guided FBDD^{26,27}. Furthermore, we designed fluorescent probes and protein degraders of PDE δ ^{28,29}, which offered new chemical tools to investigate the biological function of KRAS–PDE δ interaction. However, the known KRAS–PDE δ inhibitors are generally limited by weak *in vivo* efficacy. For example, deltarasin was unspecific to PDE δ protein, leading to a “switch-like” response to cell death. Deltazinsonone was unable to exert *in vivo* antitumor activity due to poor metabolic

stability^{20,21}. In order to identify novel KRAS–PDE δ inhibitors with enhanced antitumor potency, herein new spiro-cyclic PDE δ inhibitors were discovered from screening of an in-house library.

After structure-based hit optimization, compound **361** was identified to effectively inhibit the KRAS–PDE δ interaction and disrupt the distribution of KRAS protein. Interestingly, inhibitor **361** showed potent anti-pancreatic cancer activity both *in vitro* and *in vivo*, which represented the first KRAS–PDE δ inhibitor with *in vivo* efficacy in the patient-derived xenograft (PDX) models. Also, compound **361** is a promising lead compound for the treatment of pancreatic cancer.

2. Results and discussion

2.1. Discovery of a spiro-cyclic PDE δ inhibitor

Our in-house compound library containing diverse spiro-scaffolds^{30–33} and approved drugs was screened using the fluorescence polarization (FP) assay²⁶. First, the inhibitory ratio of all compounds was tested at 5 μ mol/L (Supporting Information Table S1). Two compounds (atorvastatin and spiperone) were identified to have an inhibitory rate over 50%. Then, the K_D value of the hit compounds was further determined. Atorvastatin has been reported to be a PDE δ inhibitor and is generally used as the probe in the FP assay¹⁷. Spiperone (**9**), which shared a spiro scaffold, exhibited moderate activity in a low micro-molar range to PDE δ ($K_D = 1471 \pm 246$ nmol/L, Fig. 2A and B). Subsequently, it was chosen for further structural optimization.

2.2. Molecular docking and drug design

In order to determine the binding mode of compound **9** towards PDE δ protein, Glide docking with extra precision (XP) was performed. According to the predicted docking pose (Fig. 2C), the amide group within the spiro scaffold of compound **9** formed a hydrogen bond to Tyr149, while the *p*-fluorobenzoyl moiety binds to the Arg61 pocket through hydrogen bonding interactions between the ketone group and Arg61 and Gln78, respectively. The docking pose exhibited an obvious hydrophobic cavity in the Arg61 pocket, which suggested that the introduction of hydrophobic groups could improve the binding affinity. Guided by the binding conformation, structure-based drug design (SBDD) was applied to design a series of new inhibitors (Fig. 2D). First,

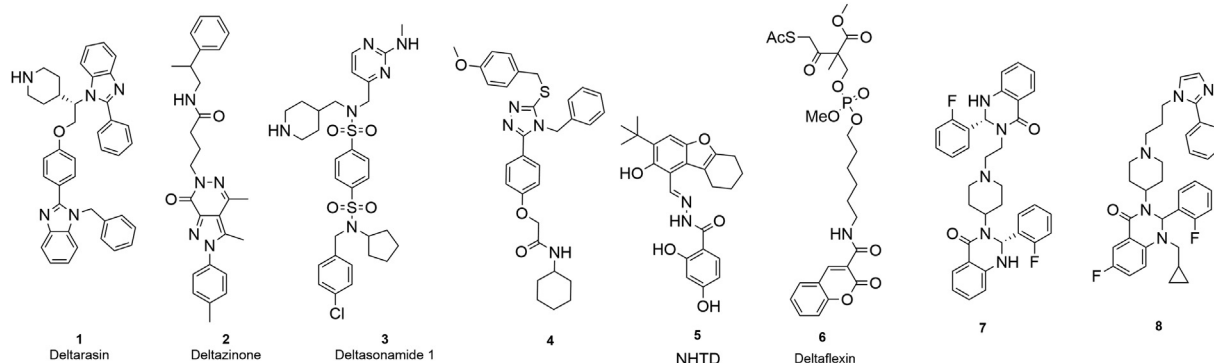


Figure 1 Chemical structures of reported KRAS–PDE δ inhibitors.

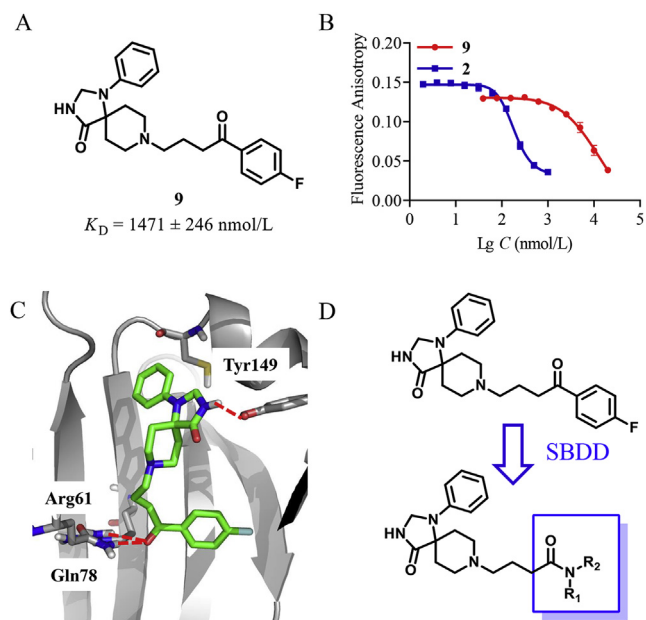


Figure 2 Discovery and optimization of spiro-cyclic PDE δ inhibitors (A) Chemical structure of compound **9** identified from an in-house library. (B) The dose–response curve for compounds **9** (red) and **2** (blue) by the FP assay; (C) The proposed binding pose of compound **9** (green) to PDE δ protein (PDB: 5X74²⁶). Hydrogen bonding interaction with Arg61, Gln78 and Tyr149 was represented by red dashed lines. (D) Optimization of compound **9** with SBDD. The figures were generated by Pymol (<http://www.Pymol.org/>).

various amides were introduced to replace the *p*-fluorobenzoyl moiety. Then *N*-monosubstitution or *N*-di-substitution was introduced by aromatic or aliphatic ring. The spiro moiety was reserved to maintain the binding conformation.

2.3. Chemistry

The synthetic route for the synthesis of target compounds **23a–23e** is shown in Scheme 1. The substituted primary amines reacted with 4-chlorobutryl chloride to give intermediates **22**, subsequently **22** reacted with intermediate **18** to afford target compounds **23a–23e**.

The synthetic route for compounds **36a–36o** is shown in Scheme 2. Reductive amination was conducted to prepare intermediates **33** with substituted aldehydes **31** and aniline **32**. Then, compounds **33** were substituted by γ -butyrolactone to obtain primary alcohols **34**, which were oxidized to aldehydes **35**. Finally, reductive amination was conducted between intermediates **35** and **18** to afford target compounds **36a–36o**.

2.4. Biological evaluations and structure–activity relationships

Initially, compounds **23a–23e** with *N*-monosubstitutions were assayed. As shown in Table 1, these compounds generally showed modest inhibitory activities (K_D range: 1538–2186 nmol/L), which were comparable to hit compound **9** ($K_D = 1471 \pm 246$ nmol/L). However, it was worth noting that introducing a large size group led to decreased PDE δ binding

affinities. For example, naphthalen-1-yl derivative **23c** showed the weakest activity ($K_D = 2186 \pm 385$ nmol/L).

When an additional phenyl group was added to the amine, most di-substituted compounds (**36**) showed comparable or superior activity to the lead compound. In particular, cyclohexyl (compound **36l**, $K_D = 127 \pm 16$ nmol/L) and cyclopentyl (compound **36m**, $K_D = 159 \pm 29$ nmol/L) derivatives showed excellent PDE δ binding affinity, which was about 7–9 fold more active than lead compound **9** ($K_D = 1471 \pm 246$ nmol/L). In contrast, less steric cyclobutyl (compound **36n**) or cyclopropyl (compound **36o**) derivative showed decreased activity. Replacement of the cycloalkyl-methyl substitutions by benzyl (**36a–36d**, K_D range: 328–1311 nmol/L) or heterocyclic methyl group (**36e–36k**, K_D range: 1240–1657 nmol/L) generally led to reduced PDE δ binding affinity. The docking result (Fig. 3A) revealed that the amide substitutions of **36l** could engage the hydrophobic pocket of PDE δ protein in which the cyclohexyl moiety formed hydrophobic interactions with residues Trp32, Val145 and Leu147. Moreover, the key hydrogen interactions with Arg61, Gln78 and Tyr149 were retained. The hydrophobic interaction between phenyl moiety and Leu38, Thr131 and Phe133 could be also observed, which was absent in the docking pose of compound **9** (Fig. 3B).

Furthermore, *in vitro* antitumor activity of the target compounds was assayed against human pancreatic cancer cell line Mia PaCa-2 (Table 1). PDE δ inhibitors **9** and **2** failed to exert cellular potency ($IC_{50} > 100$ μ mol/L). Interestingly, most target compounds showed moderate to good antitumor activity. Among them, compound **36l** ($K_D = 127 \pm 16$ nmol/L, $IC_{50} = 6.3 \pm 1.7$ μ mol/L) possessed balanced inhibitory activity both at the molecular and cellular level. Furthermore, patient-driven primary cells 098 and 099 were applied to evaluate the potential clinical application of compound **36l** (Fig. 4). The 098 and 099 were both KRAS^{G12D} mutant pancreatic cancer cells. The result showed that **36l** (IC_{50} range: 6.4–7.6 μ mol/L) exhibited potent activity against primary pancreatic cancer cell line, while compound **2** ($IC_{50} > 100$ μ mol/L) was totally inactive. Moreover, water solubility of inhibitor **36l** (0.63 mmol/L) was about 20 fold higher than compound **2** (0.030 mmol/L). Considering the activity and physicochemical properties, compound **36l** was chosen for further biological evaluations.

2.5. The cellular thermal shift assay (CETSA)

The CETSA assay is a useful method for the discovery of the intracellular target of inhibitors. The method evaluates the change in the stability when protein binds with the small molecules, which is fast and convenient without purifying the protein^{34,35}. Mia Paca-2 cells were treated by compound **36l** at 20 and 50 μ mol/L, respectively, using compound **2** as a positive drug (Fig. 5A). Increased T_{agg} (aggregation temperature) values were observed in the group treated by compounds **2** and **36l**. In addition, compound **36l** introduced a higher T_{agg} value change than that of compound **2** at 50 μ mol/L. The experiment verified PDE δ protein was the target of compound **36l** in Mia Paca-2 cells.

2.6. Co-immunoprecipitation (Co-IP) experiment

Co-IP is a powerful technique for the identification of protein–protein interaction^{36,37}. Co-IP experiment was further conducted

to evaluate the inhibition of KRAS–PDE δ by compound **361** (Fig. 5B). The cells were treated with compound **361** at 20 $\mu\text{mol/L}$ for 24 h. Western blotting experiment was used to identify KRAS and PDE δ protein, respectively. The level of PDE δ /KRAS in the **361** treating group was lower than the control group. The results confirmed that the compound **361** effectively disrupted the interaction of KRAS–PDE δ .

2.7. Compound **361** inhibited the phosphorylation of AKT in Mia PaCa-2 cells

The mutant KRAS protein activates downstream signal pathways, such as RAS-RAF-MAPK and PI3K-AKT-mTOR pathway, and then stimulates the growth, proliferation, and differentiation of cancer cells¹⁸. Thus, the effects of compound **361** on the phosphorylation of total extracellular signal-regulated kinase (t-ERK) and protein kinase B (t-AKT) were evaluated. Based on our previous work²⁹, the epidermal growth factor (EGF) was applied to induce the expression and phosphorylation of t-ERK and t-AKT. Phosphorylation levels were determined by treating Mia PaCa-2 cells with compounds **361** for 4 h followed by stimulating for another 10 min with EGF. Compound **2** was used as positive control. As shown in Fig. 6, compounds **361** interfered with phosphorylation of t-ERK and t-AKT in a dose-dependent manner in Mia PaCa-2 cells, and significantly reduced their phosphorylation at 100 $\mu\text{mol/L}$, which was more potent than that of positive compound **2**.

2.8. Compound **361** increased KRAS-dependent apoptosis and influenced the distribution of KRAS protein in Mia PaCa-2 cells

The results of apoptosis assay demonstrated that positive control **2** induced cell apoptosis with an apoptotic rate of 28.55% at 50 $\mu\text{mol/L}$ and 38.32% at 100 $\mu\text{mol/L}$ respectively (Fig. 7). Similarly, compound **361** effectively promoted apoptosis of Mia PaCa-2 cells, and induced apoptosis in 19.42%, 31.22% and 54.28% at 5, 10 and 20 $\mu\text{mol/L}$, respectively. The results suggested that both compounds **2** and **361** induced apoptosis in a dose-dependent manner. Spiro-cyclic inhibitor **361** was more potent even at a lower concentration. Immunofluorescence staining was further applied to evaluate the KRAS distribution in Mia PaCa-2 cells (Fig. 8). Compound **361** was observed to accumulate PDE δ around the cell nucleus and disrupt the distribution of KRAS to endomembrane at 20 $\mu\text{mol/L}$, while compound **2** showed similar effects at the higher concentration (100 $\mu\text{mol/L}$).

2.9. Compound **361** inhibited proliferation of the pancreatic tumor in patient-derived xenograft (PDX) model

In order to evaluate the *in vivo* anti-pancreatic tumor activity, patient-derived primary cell lines were applied to detect the anti-proliferative effects of compound **361** (Fig. 9). Four KRAS mutant clinical primary pancreatic cancer cell lines [0001 (*KRAS*^{G12A}), 0034 (*KRAS*^{G12R}), 0037 (*KRAS*^{G12D}) and 0043 (*KRAS*^{G12D})] were treated with **361** at different time. The results revealed that compound **361** dose-dependently inhibited the growth of primary cell lines. Moreover, 0001, 0037 and 0034 cell lines were more sensitive to inhibitor **361** than the 0043 cell line. Pharmacokinetic study and cellular permeability of **361** were further conducted in ICR mice. The results indicated that the spiro-cyclic inhibitor **361** exhibited acceptable plasma exposures ($C_{\text{max}} = 15.50 \mu\text{g/mL}$,

$\text{AUC}_{0-t} = 59.23 \text{ h}\cdot\mu\text{g/mL}$) and moderate cellular permeability (Supporting Information Fig. S1 and Table S3), which enabled further *in vivo* studies.

Based on the cellular potency of inhibitor **361**, PDX models were further applied to evaluate the *in vivo* antitumor potency. Guided by the antiproliferative assay to primary cells, the excised tumor tissue of patients produced 0034 primary cells was implanted into nude female mice. Consideration of the metabolic instability of compound **2**, gemcitabine, a cytotoxic antitumor agent, was chosen as the positive drug. As depicted in Fig. 9, Compound **361** significantly inhibited the tumor growth with the tumor growth inhibition (TGI) rate of 57.3% (Fig. 10A and B). Moreover, the significant difference of tumor weight was also observed between compound **361** and the control group (Fig. 10C). Despite that the *in vivo* antitumor activity of compound **361** was lower than cytotoxic antitumor agent gemcitabine, it was the first KRAS–PDE δ inhibitor with potent antitumor efficacy in PDX models. To further validate the *in vivo* antitumor potency, compound **361** (25, 50 and 75 mg/kg, QD) and positive control **2** (50 mg/kg, QD) were evaluated in Mia PaCa-2 pancreatic cancer mouse xenograft models. In consistent with the results from PDX models, compound **361** dose dependently inhibited the tumor growth without obvious adverse effects (Supporting Information Fig. S2). These results highlighted the therapeutic potential of this new class of PDE δ inhibitors in treating pancreatic cancer.

Furthermore, hematoxylin-eosin (H&E) staining and immunohisto-chemistry (IHC) for Ki-67 was performed for the investigation of the action mechanism of inhibitor **361** against the pancreatic tumor *in vivo*. As shown in Fig. 10D and E, hyalini-zation and reduction of cellularity was observed in the tumor treated with compound **361** (marked by dark arrow respectively) in the images of H&E staining and magnification image, while decreased proliferation was exhibited as shown by Ki-67 immunostaining. The same variation was visible in the gemcitabine group. The results supported the *in vivo* efficacy of **361**.

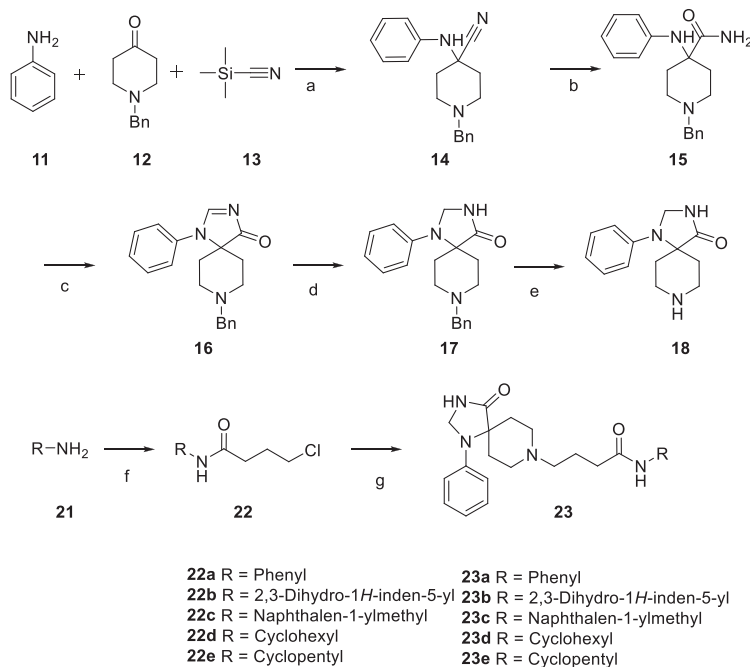
3. Conclusions

In summary, new spiro-cyclic KRAS–PDE δ inhibitors were discovered by screening an in-house compound library and structure-based hit optimization. As compared with the hit compound, inhibitor **361** showed improved PDE δ binding affinity and antitumor activity. In KRAS-dependent Mia PaCa-2 cells, compound **361** promoted the apoptosis, induced down-regulation of t-AKT phosphorylation and disrupted the diffusion of KRAS in the cytoplasm. The spiro-cyclic KRAS–PDE δ inhibitors revealed remarkable advantages over known ones due to the potent anti-tumor activity both *in vitro* and *in vivo*. In particular, compound **361** showed good therapeutic efficacy in the pancreatic cancer PDX models. Taken together, this study provides a promising lead compound for investigating the druggability of KRAS–PDE δ protein–protein interaction. Further structural optimization of the spiro-cyclic inhibitors is in progress.

4. Experimental

4.1. Chemistry

All reagents were commercially available and used without further purification. ¹H NMR and ¹³C NMR spectra were recorded on



Scheme 1 Reagent and conditions: (a) AcOH, rt, 2.5 h; (b) 98% H₂SO₄, rt, 18 h; (c) DMF-DMA, MeOH, 55 °C, 16 h; (d) NaBH₄, MeOH, rt, 2 h; (e) H₂, 20% Pd(OH)₂, MeOH, rt, overnight; (f) 4-Chlorobutyl chloride, TEA, DCM, rt, 2 h; (g) **18**, TEA, KI, acetonitrile, 90 °C, 24 h.

Bruker AVANCE300 or AVANCE600 spectrometer (Bruker Company, Germany). CDCl₃ or DMSO-*d*₆ were solvents with TMS as an internal standard. Chemical shifts (δ values) and coupling constants (*J* values) are given in ppm and Hz, respectively. HRMS spectra were detected on an Esquire 3000 LC-MS mass spectrometer. Precoated plates GF-254 (Qingdao Haiyang Chemical, China) and silica gel 60G (Qingdao Haiyang Chemical) were adopted for monitoring reaction and column chromatography respectively. The purities of final compounds were analyzed by HPLC (Agilent 1260), and were greater than 95%.

4.1.1. 1-Phenyl-1,3,8-triazaspiro[4.5]decan-4-one (**18**)

The synthesis of intermediate **18** was according to the literature³⁹. White solid. ¹H NMR (600 MHz, DMSO-*d*₆) δ 8.91 (s, 1H), 7.21 (dd, 2H, *J* = 7.5, 8.7 Hz), 6.98 (d, 2H, *J* = 8.2 Hz), 6.76 (t, 1H, *J* = 7.5 Hz), 4.60 (s, 2H), 3.43–3.48 (m, 2H), 3.18–3.21 (m, 2H), 3.69–2.75 (m, 2H), 1.73 (d, 2H, *J* = 14.2 Hz).

4.1.2. 4-Chloro-*N*-phenylbutanamide (**22a**)

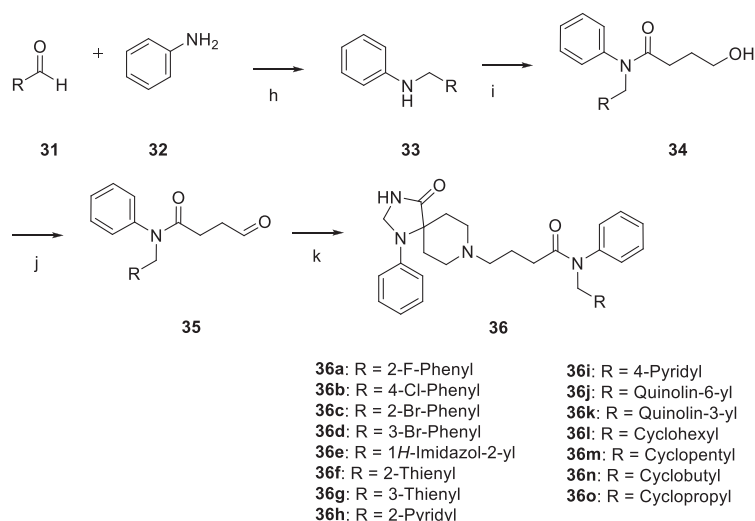
A mixture of aniline **21a** (470 mg, 1 eq, 5 mmol), 4-chlorobutyl chloride (850 mg, 1.2 eq, 6 mmol), TEA (1.01 g, 2eq, 10 mmol) in DCM (20 mL) was reacted at room temperature for 2 h. The mixture was washed with saturated Na₂CO₃ solution. The organic layer was combined and washed with brine, then it was evaporated to afford the crude product. Intermediate **22a** was purified by flash column chromatography (hexane/ethyl acetate = 75:25) as white solid (yield 51.4%). ¹H NMR (300 MHz, DMSO-*d*₆) δ 9.98 (s, 1H), 7.59 (d, 2H, *J* = 7.7 Hz), 7.28 (t, 2H, *J* = 7.7 Hz), 7.02 (t, 1H, *J* = 7.7 Hz), 3.70 (t, 2H, *J* = 6.8 Hz), 2.48 (t, 2H, *J* = 6.8 Hz), 1.98–2.07 (m, 2H).

4.1.3. 4-(4-Oxo-1-phenyl-1,3,8-triazaspiro[4.5]decan-8-yl)-*N*-phenylbutanamide (**23a**)

Intermediate **22a** (400 mg, 2 eq, 2 mmol), **18** (230 mg, 1 eq, 1 mmol) and KI (17 mg, 0.1 eq, 0.1 mmol) were added into acetonitrile (10 mL) and reacted under reflux. Additional **22a** (1 eq, 1 mmol) was added to the reaction 2 h later. The mixture was reacted for another 24 h under reflux, and then concentrated under reduced pressure and purified by flash column chromatography (dichloromethane/methanol = 100:7) to give target molecules **23a** (yield 36.4%). ¹H NMR (600 MHz, DMSO-*d*₆) δ 10.02 (s, 1H), 8.69 (s, 1H), 7.52 (d, 2H, *J* = 8.8 Hz), 7.27 (t, 2H, *J* = 8.2 Hz), 7.20 (t, 2H, *J* = 8.2 Hz), 7.11 (t, 1H, *J* = 7.2 Hz), 6.87 (d, 2H, *J* = 8.2 Hz), 6.78 (t, 1H, *J* = 7.6 Hz), 4.57 (s, 2H), 3.18 (br, 4H), 2.78 (t, 2H, *J* = 7.6 Hz), 2.61–2.66 (m, 2H), 2.37 (t, 2H, *J* = 6.9 Hz), 1.85–1.90 (m, 2H), 1.73 (d, 2H, *J* = 14.4 Hz). ¹³C NMR (150 MHz, DMSO-*d*₆) δ 176.46, 171.46, 143.75, 139.81, 129.47, 129.10, 123.37, 119.50, 118.16, 114.79, 59.14, 58.51, 57.49, 49.59, 34.69, 28.48, 22.53. HRMS: *m/z* calcd. for C₂₃H₂₈N₄O₂ 392.2212, found 393.2270 [M+H]⁺. HPLC purity: 95.3%, *t*_R = 8.942 min.

4.1.4. *N*-(2,3-Dihydro-1*H*-inden-5-yl)-4-(4-oxo-1-phenyl-1,3,8-triazaspiro[4.5]decan-8-yl)butanamide (**23b**)

Pale solid, 135 mg, yield 31.3%. Synthesized by the protocol of compound **23a** with **22b** (475 mg, 2 mmol), **18** (230 mg, 1 mmol) and KI (17 mg, 0.1 mmol) and purified by flash column chromatography (dichloromethane/methanol = 100:7). ¹H NMR (600 MHz, DMSO-*d*₆) δ 9.82 (s, 1H), 8.74 (s, 1H), 7.52 (s, 1H), 7.28 (d, 1H, *J* = 7.9 Hz), 7.20 (t, 2H, *J* = 7.9 Hz), 7.11 (d, 1H, *J* = 7.9 Hz), 6.89 (d, 2H, *J* = 7.9 Hz), 6.75 (t, 1H, *J* = 7.9 Hz),



Scheme 2 Reagents and conditions: (h) MgSO₄, NaBH₄, MeOH, rt, overnight; (i) γ -butyro-lactone, trimethylaluminum, toluene, 80 °C, 12 h; (j) DMP, DCM, rt, 2 h; (j) **18**, MgSO₄, NaBH₄, MeOH, rt, overnight.

4.58 (s, 2H), 3.02 (br, 4H), 2.71–2.81 (m, 4H), 2.63–2.68 (m, 4H), 2.36 (t, 2H, $J = 7.9$ Hz), 1.96–2.01 (m, 2H), 1.84–1.86 (m, 2H), 1.67 (d, 2H, $J = 13.3$ Hz). ¹³C NMR (150 MHz, DMSO-*d*₆) δ 176.20, 170.94, 144.47, 143.65, 138.59, 137.97, 129.50, 124.52, 118.27, 117.73, 115.81, 114.82, 59.20, 58.20, 57.15, 49.43, 34.39, 32.98, 32.23, 27.99, 25.64, 21.99. HRMS: m/z calcd. for C₂₆H₃₂N₄O₂ 432.2525, found 433.2606 [M+H]⁺. HPLC purity: 99.1%, $t_R = 12.394$ min.

4.1.5. *N*-(Naphthalen-1-ylmethyl)-4-(4-oxo-1-phenyl-1,3,8-triazaspiro[4.5]decan-8-yl)butanamide (**23e**)

Pale solid, 129 mg, yield 28.2%. Synthesized by the protocol of compound **23a** with **22c** (522 mg, 2 mmol), **18** (230 mg, 1 mmol) and KI (17 mg, 0.1 mmol) and purified by flash column chromatography (dichloromethane/methanol = 100:7). ¹H NMR (600 MHz, DMSO-*d*₆) δ 8.79 (s, 1H), 8.43 (t, 1H, $J = 5.3$ Hz), 8.08 (d, 1H, $J = 8.8$ Hz), 7.95 (d, 1H, $J = 7.0$ Hz), 7.85–7.86 (m, 1H), 7.53–7.59 (m, 2H), 7.45–7.49 (m, 2H), 7.22 (t, 2H, $J = 7.9$ Hz), 6.90 (d, 2H, $J = 8.8$ Hz), 6.76 (d, 1H, $J = 7.9$ Hz), 4.76 (d, 2H, $J = 5.3$ Hz), 4.60 (s, 2H), 3.03 (br, 4H), 2.64–2.68 (m, 4H), 2.25 (t, 2H, $J = 6.1$ Hz), 1.81–1.86 (m, 2H), 1.68 (d, 2H, $J = 14.1$ Hz). ¹³C NMR (150 MHz, DMSO-*d*₆) δ 175.70, 171.54, 143.16, 134.71, 133.32, 130.91, 129.02, 128.50, 127.58, 126.21, 125.79, 125.61, 125.38, 123.52, 117.86, 114.34, 58.74, 57.63, 56.49, 48.79, 40.23, 32.83, 27.39, 21.58. HRMS: m/z calcd. for C₂₈H₃₂N₄O₂ 456.2525, found 457.2604 [M+H]⁺. HPLC purity: 99.3%, $t_R = 11.154$ min.

4.1.6. *N*-Cyclohexyl-4-(4-oxo-1-phenyl-1,3,8-triazaspiro[4.5]decan-8-yl)butanamide (**23d**)

White solid, 142 mg, yield 35.7%. Synthesized by the protocol of compound **23a** with **22d** (410 mg, 2 mmol), **18** (230 mg, 1 mmol) and KI (17 mg, 0.1 mmol) and purified by flash column chromatography (dichloromethane/methanol = 100:7). ¹H NMR (600 MHz, DMSO-*d*₆) δ 8.73 (s, 1H), 7.70 (d, 1H, $J = 7.6$ Hz), 7.25 (d, 2H, $J = 8.2$ Hz), 6.90 (d, 2H, $J = 8.2$ Hz), 6.78 (t, 1H, $J = 7.2$ Hz), 4.6 (s, 2H), 3.52–3.55 (m, 1H), 2.91–2.93 (m, 4H),

2.62–2.64 (m, 2H), 2.11 (t, 2H, $J = 8.7$ Hz), 1.55–1.75 (m, 9H), 1.23–1.29 (m, 2H), 1.09–1.17 (m, 3H). ¹³C NMR (150 MHz, CDCl₃) δ 176.39, 171.24, 143.77, 129.55, 118.31, 114.87, 59.24, 58.38, 57.32, 49.48, 47.90, 33.70, 33.05, 28.26, 25.79, 25.14, 22.61. HRMS: m/z calcd. for C₂₃H₃₄N₄O₂ 398.2782, found 399.2763 [M+H]⁺. HPLC purity: 99.2%, $t_R = 9.850$ min.

4.1.7. *N*-Cyclopentyl-4-(4-oxo-1-phenyl-1,3,8-triazaspiro[4.5]decan-8-yl)butanamide (**23e**)

Pale solid, 135 mg, yield 35.2%. Synthesized by the protocol of compound **23a** with **22e** (380 mg, 2 mmol), **18** (230 mg, 1 mmol) and KI (17 mg, 0.1 mmol) and purified by flash column chromatography (dichloromethane/methanol = 100:7). ¹H NMR (600 MHz, DMSO-*d*₆) δ 8.71 (s, 1H), 7.78 (d, 1H, $J = 7.6$ Hz), 7.25 (t, 2H, $J = 7.6$ Hz), 6.90 (d, 2H, $J = 7.6$ Hz), 6.78 (t, 1H, $J = 7.6$ Hz), 4.60 (s, 2H), 3.98–4.01 (m, 1H), 2.86–2.90 (m, 4H), 2.58–2.63 (m, 2H), 2.47–2.50 (m, 2H), 2.10 (t, 2H, $J = 7.6$ Hz), 1.77–1.81 (m, 2H), 1.70–1.75 (m, 2H), 1.60–1.65 (m, 4H), 1.49–1.51 (m, 2H), 1.33–1.39 (m, 2H). ¹³C NMR (150 MHz, DMSO-*d*₆) δ 176.39, 171.70, 143.74, 129.49, 118.26, 114.85, 59.171, 58.402, 57.402, 50.624, 49.491, 33.625, 32.773, 28.338, 23.905, 22.686. HRMS: m/z calcd. for C₂₂H₃₂N₄O₂ 384.2525, found 385.2602 [M+H]⁺. HPLC purity: 98.9%, $t_R = 9.887$ min.

4.1.8. *N*-(2-Fluorobenzyl)aniline (**33a**)

The synthesis of secondary amines **33a** was applied the reductive amination procedure according to the literature procedure I²². In brief, a solution of 2-fluorobenzaldehyde **31a** (465 mg, 1 eq, 5 mmol) and aniline **32** (0.47 g, 1 eq, 5 mmol) in methanol (25 mL) was treated with MgSO₄ (1.2 g, 10 mmol) at room temperature overnight. Sodium borohydride (95 mg, 0.5 eq, 2.5 mmol) was added into the reaction under ice bath and reacted for another 2 h. The mixture was filtered. The methanol kept and removed *in vacuo* to give the secondary amines. The product **33a** (825 mg) was used directly in the next step without purification. ¹H NMR (300 MHz, DMSO-*d*₆) δ 7.35 (t, 1H, $J = 7.5$ Hz), 7.22–7.29 (m, 1H), 7.08–7.17 (m, 2H), 7.01 (t, 2H, $J = 7.8$ Hz),

6.46–6.55 (m, 2H), 6.16 (t, 2H, $J = 5.9$ Hz), 4.26 (d, 2H, $J = 6.2$ Hz).

4.1.9. *N*-(2-Fluorobenzyl)-4-hydroxy-*N*-phenylbutanamide (34a)

The secondary amines **33a** (600 mg, 1 eq, 3 mmol) was dissolved into dry toluene (10 mL) and protected by nitrogen. The reaction was cooled down to 0 °C, and trimethylaluminum (2 mol/L in toluene, 2 eq, 3 mL) was added to the solution dropwise. The mixture was reacted for 2 h and γ -butyrolactone (510 mg, 2 eq, 6 mmol) was added. The solution was reacted at 65 °C for 24 h. The reaction mixture was moved to ice bath. Then, methanol (5 mL) was added dropwise followed by saturated sodium tartrate solution. Ethyl acetate (30 mL) was used to wash the solution and combined. The crude product was afforded by removing the ethyl acetate and purified by flash column chromatography (hexane/ethyl = 40:60–0:100) to give intermediate **34a** (105 mg, 12.2% yield). ¹H NMR (300 MHz, DMSO-*d*₆) δ 7.05–7.39 (m, 9H), 4.90 (s, 2H), 4.36 (t, 1H, $J = 5.1$ Hz), 3.28 (t, 2H, $J = 6.3$ Hz), 2.08 (t, 2H, $J = 7.2$ Hz), 1.57–1.66 (m, 2H).

4.1.10. *N*-(2-Fluorobenzyl)-4-oxo-*N*-phenylbutanamide (35a)

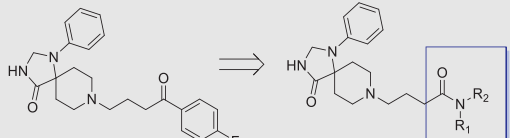
A solution of **34a** (145 mg, 1 eq, 0.5 mmol) in dry DCM (15 mL) were stirred at 0 °C added Dess–Martin reagent (425 mg, 2 eq, 1 mmol). The resulting suspension was reacted for 1 h at room temperature. After completion of the reaction, the solution was

added saturated sodium thiosulfate solution followed by saturated Na₂CO₃ solution. The water phase was washed with DCM twice. The organic layer was combined, washed with brine and evaporated under reduced pressure to afford crude product. The crude product was purified by column chromatography (hexane/ethyl = 75:25) to give target molecules **35a** (86 mg, 60.3% yield). ¹H NMR (300 MHz, DCCl₃) δ 9.80 (s, 1H), 7.31–7.37 (m, 4H), 7.17–7.22 (m, 1H), 7.05–7.10 (m, 3H), 6.92 (t, 1H, $J = 8.8$ Hz), 4.96 (s, 2H), 2.78 (t, 2H, $J = 6.4$ Hz), 2.36 (t, 2H, $J = 6.4$ Hz).

4.1.11. *N*-(2-Fluorobenzyl)-4-(4-oxo-1-phenyl-1,3,8-triazaspiro[4.5]decan-8-yl)-*N*-phenylbutanamide (36a)

Target compounds **36a** were prepared by the reductive amination by using **35a** (142 mg, 1 eq, 0.5 mmol), **18** (115 mg, 1 eq, 0.5 mmol) and MgSO₄ (300 mg, 2.5 mmol) in dry methanol (10 mL) as the procedure of preparation of **33a**. The product was purified by flash C18 column chromatography [H₂O (0.1% TFA)/methanol = 40:60–80:20] to give target molecules **36a** (pale solid, 76 mg, yield 30.4%). ¹H NMR (600 MHz, DMSO-*d*₆) δ 8.60 (s, 1H), 7.32–7.35 (m, 3H), 7.24–7.27 (m, 2H), 7.18–7.21 (m, 4H), 7.11–7.13 (m, 1H), 7.06–7.09 (m, 1H), 6.75–6.78 (m, 3H), 4.91 (s, 2H), 4.55 (s, 2H), 2.58 (br, 4H), 2.35–2.40 (m, 2H), 2.21 (t, 2H, $J = 6.9$ Hz), 2.11 (t, 2H, $J = 6.7$ Hz), 1.65–1.67 (m, 2H), 1.59 (d, 2H, $J = 13.5$ Hz). ¹³C NMR (150 MHz, DMSO-*d*₆) δ 163.53, 161.33, 159.69, 157.18, 153.61, 147.75, 135.13, 135.01, 134.64, 132.52, 131.97, 131.92, 131.29, 130.27, 129.67, 129.44.

Table 1 Structures, binding affinity and anti-pancreatic cancer activities of PDE δ inhibitors.



Compd.	R ₁	R ₂	PDE δ ^a (K_D , nmol/L)	Mia PaCa-2 ^b (IC ₅₀ , μ mol/L)
23a	H	Ph	1670 \pm 260	46 \pm 14
23b	H	2,3-Dihydro-1 <i>H</i> -inden-5-yl	1538 \pm 166	3.6 \pm 2.1
23c	H	Naphthalen-1-ylmethyl	2186 \pm 385	4.8 \pm 1.2
23d	H	Cyclohexyl	1699 \pm 178	64 \pm 8.1
23e	H	Cyclopentyl	1543 \pm 244	>100
36a	Ph	2-F-Benzyl	1311 \pm 219	16 \pm 0.10
36b	Ph	4-Cl-Benzyl	328 \pm 59	4.3 \pm 2.1
36c	Ph	2-Br-Benzyl	485 \pm 35	12 \pm 0.60
36d	Ph	3-Br-Benzyl	690 \pm 198	4.9 \pm 1.4
36e	Ph	1 <i>H</i> -Imidazole-4-ylmethyl	1657 \pm 436	>100
36f	Ph	Thiophen-2-ylmethyl	1475 \pm 197	15 \pm 5.4
36g	Ph	Thiophen-3-ylmethyl	1240 \pm 106	17 \pm 8.3
36h	Ph	Pyridin-2-ylmethyl	1373 \pm 317	46 \pm 21
36i	Ph	Pyridin-4-ylmethyl	1482 \pm 18	55 \pm 2.8
36j	Ph	Quinolin-6-ylmethyl	1343 \pm 36	12 \pm 4.0
36k	Ph	Quinolin-3-ylmethyl	1328 \pm 32	13 \pm 2.8
36l	Ph	Cyclohexylmethyl	127 \pm 16	6.7 \pm 1.7
36m	Ph	Cyclopentylmethyl	159 \pm 29	18 \pm 1.5
36n	Ph	Cyclobutylmethyl	393 \pm 27	19 \pm 4.0
36o	Ph	Cyclopropylmethyl	1125 \pm 140	26 \pm 1.6
9	/	/	1471 \pm 246	>100
2	/	/	34 \pm 4	>100

^aTested by fluorescent anisotropy assay.

^bTested by the CCK8 method.

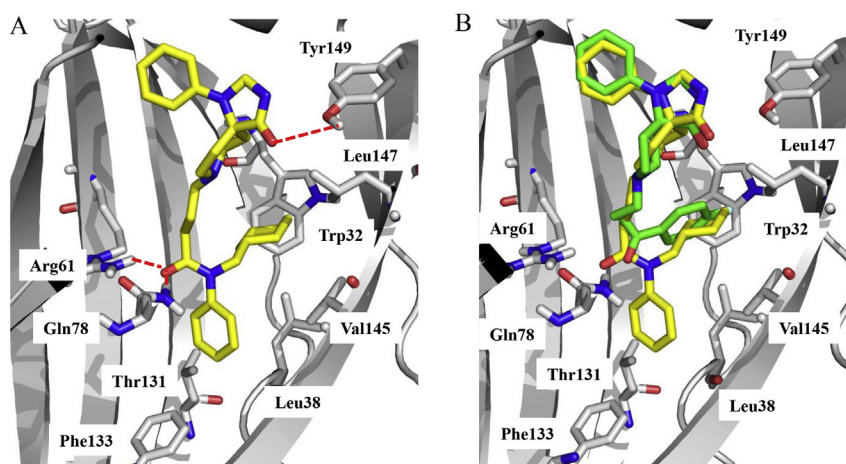


Figure 3 Molecular docking of **361** with PDE δ protein. (A) Proposed-bonding mode of **361** with PDE δ protein. The red dash line represented hydrogen interaction with residues Arg61, Gln78 and Tyr149. (B) The overlay image binding mode of compounds **361** (yellow) and **9** (green) with PDE δ protein.

129.10, 128.57, 128.48, 125.77, 125.65, 118.80, 117.96, 117.10, 116.96, 115.86, 115.82, 115.53, 114.00, 69.18, 66.93, 45.82. MS (ESI): m/z calcd. for $C_{30}H_{33}FN_4O_2$ 500.2588, found 501.2658 $[M+H]^+$. HPLC purity: 98.7%, t_R = 13.036 min.

4.1.12. *N*-(4-Chlorobenzyl)-4-(4-oxo-1-phenyl-1,3,8-triazaspiro [4.5]decan-8-yl)-*N*-phenylbutanamide (36b**)**

Pale solid, 86 mg, yield 33.2%. Synthesized by the protocol of compound **36a** with **35b** (150 mg, 0.5 mmol) and **18** (115 mg, 0.5 mmol) and purified by flash C18 column chromatography [H_2O (0.1% TFA)/methanol = 40:60–80:20]. 1H NMR (600 MHz, $DMSO-d_6$) δ 8.65 (s, 1H), 7.34–7.39 (m, 4H), 7.30 (t, 1H, J = 7.1 Hz), 7.18–7.24 (m, 6H), 6.78–6.82 (m, 3H), 4.86 (s, 2H), 4.58 (s, 2H), 2.71 (d, 4H, J = 7.8 Hz), 2.41–2.46 (m, 2H), 2.23 (t, 2H, J = 6.5 Hz), 2.14 (t, 2H, J = 8.4 Hz), 1.69–1.74 (m, 2H), 1.56 (d, 2H, J = 13.6 Hz). ^{13}C NMR (150 MHz, $DMSO-d_6$) δ 176.00, 171.88, 143.28, 142.14, 136.79, 131.62, 129.82, 129.48, 128.98, 128.27, 128.16, 117.83, 114.48, 58.64, 58.08, 56.64, 51.30, 48.97, 31.23, 28.08, 22.12. HRMS (ESI): m/z calcd. for $C_{30}H_{33}ClN_4O_2$ 516.2292, found 517.2381 $[M+H]^+$. HPLC purity: 96.9%, t_R = 14.829 min.

4.1.13. *N*-(2-Bromobenzyl)-4-(4-oxo-1-phenyl-1,3,8-triazaspiro [4.5]decan-8-yl)-*N*-phenylbutanamide (36c**)**

Yellow solid, 99 mg, yield 35.3%. Synthesized by the protocol of compound **36a** with **35c** (172 mg, 0.5 mmol) and **18** (115 mg, 0.5 mmol) and purified by flash C18 column chromatography [H_2O (0.1% TFA)/methanol = 50:50–80:20]. 1H NMR (600 MHz, $DMSO-d_6$) δ 8.62 (s, 1H), 7.55 (d, 1H, J = 8.1 Hz), 7.27–7.39 (m, 7H), 7.16–7.22 (m, 3H), 6.76–6.79 (m, 3H), 4.93 (s, 2H), 4.56 (s, 2H), 2.56–2.59 (m, 4H), 2.36–2.41 (m, 2H), 2.24 (t, 2H, J = 7.1 Hz), 2.18 (t, 2H, J = 7.7 Hz), 1.66–1.71 (m, 2H), 1.56 (d, 2H, J = 14.1 Hz). ^{13}C NMR (150 MHz, $DMSO-d_6$) δ 176.15, 172.05, 143.34, 142.17, 136.13, 132.47, 129.71, 129.41, 129.09, 128.96, 128.04, 127.73, 122.58, 117.71, 114.40, 58.61, 58.29, 56.82, 52.20, 49.11, 48.58, 31.22, 28.42, 22.47. HRMS (ESI): m/z calcd. for $C_{30}H_{33}BrN_4O_2$ 560.1787, found 561.1846 $[M+H]^+$. HPLC purity: 99.3%, t_R = 14.700 min.

4.1.14. *N*-(3-Bromobenzyl)-4-(4-oxo-1-phenyl-1,3,8-triazaspiro [4.5]decan-8-yl)-*N*-phenylbutanamide (36d**)**

Yellow solid, 101 mg, yield 36.3%. Synthesized by the protocol of compound **36a** with **35d** (172 mg, 0.5 mmol) and **18** (115 mg,

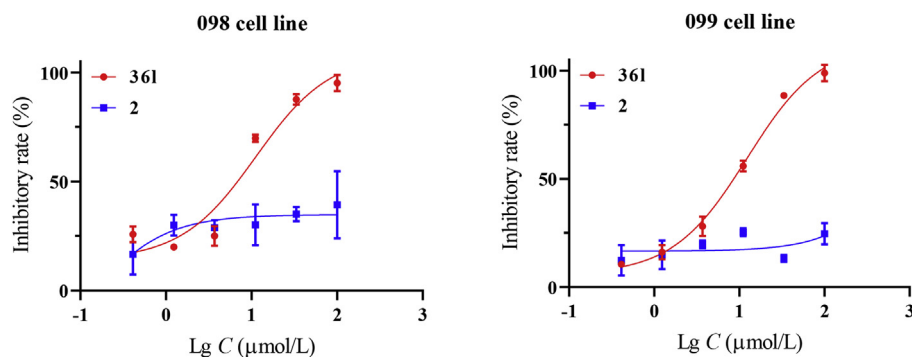


Figure 4 *In vitro* inhibitory activity of compound **361** against two clinical pancreatic cancer cell lines. The primary cell lines 098 and 099 ($KRAS^{G12D}$ mutation) were treated with **361** at various concentrations for 72 h. The percentages of viability were measured by CCK8 method. The studies with primary cell lines were approved by the Changhai Hospital Ethics Committee. Data were represented as means \pm SEM, n = 3.

0.5 mmol) and purified by flash C18 column chromatography [H₂O (0.1% TFA)/methanol = 50:50–80:20]. ¹H NMR (600 MHz, DMSO-*d*₆) δ 8.59 (s, 1H), 7.42 (d, 1H, *J* = 8.0 Hz), 7.35–7.37 (m, 3H), 7.28 (t, 1H, *J* = 7.4 Hz), 7.25 (t, 1H, *J* = 7.9 Hz), 7.18–7.21 (m, 5H), 6.75–6.78 (m, 3H), 4.84 (s, 2H), 4.54 (s, 2H), 2.55–2.60 (m, 4H), 2.34–2.39 (m, 2H), 2.22 (t, 2H, *J* = 7.8 Hz), 2.13 (t, 2H, *J* = 6.8 Hz), 1.64–1.69 (m, 2H), 1.50 (d, 2H, *J* = 13.2 Hz). ¹³C NMR (150 MHz, DMSO-*d*₆) δ 176.15, 172.05, 143.34, 142.17, 141.12, 130.96, 130.40, 129.95, 129.43, 128.55, 128.21, 127.37, 122.02, 118.26, 114.99, 59.08, 58.75, 57.26, 51.87, 49.58, 31.68, 28.88, 22.96. HRMS (ESI): *m/z* calcd. for C₃₀H₃₃BrN₄O₂ 560.1787, found 561.1865 [M+H]⁺. HPLC purity: 97.9%, *t*_R = 14.361 min.

4.1.15. *N*-((1*H*-Imidazole-4-yl)methyl)-4-(4-oxo-1-phenyl-1,3,8-triazaspiro[4.5]decan-8-yl)-*N*-phenylbutanamide (36e)

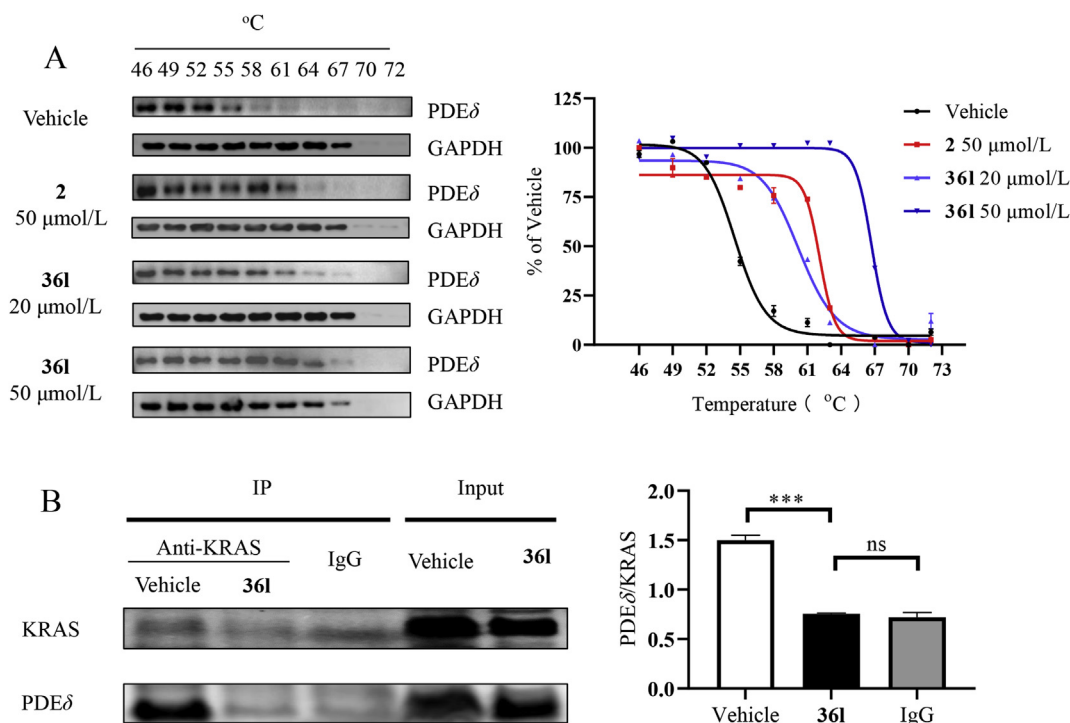
Yellow solid, 61 mg, yield 25.8%. Synthesized by the protocol of compound **36a** with **35e** (129 mg, 0.5 mmol) and **18** (115 mg, 0.5 mmol) and purified by flash C18 column chromatography [H₂O (0.1% TFA)/methanol = 50:50–80:20]. ¹H NMR (600 MHz, DMSO-*d*₆) δ 8.97 (s, 1H), 7.20–7.40 (m, 7H), 6.94–6.99 (m, 4H), 6.78 (t, 1H, *J* = 7.5 Hz), 4.89 (s, 2H), 4.62 (s, 2H), 3.31–3.43 (m, 4H), 2.79–2.95 (m, 4H), 2.16 (br, 2H), 1.90 (br, 2H), 1.79 (d, 2H, *J* = 14.2 Hz). ¹³C NMR (150 MHz, DMSO-*d*₆) δ 175.58, 171.52, 144.01, 143.34, 142.44, 129.95, 129.53, 128.64, 128.38, 122.23, 118.43, 114.71, 59.29, 57.42, 56.01, 48.79, 46.59, 31.46, 26.72, 20.18. HRMS (ESI): *m/z* calcd. for C₂₇H₃₂N₆O₂ 472.2587, found 473.2679 [M+H]⁺. HPLC purity: 98.0%, *t*_R = 7.85 min.

4.1.16. 4-(4-Oxo-1-phenyl-1,3,8-triazaspiro[4.5]decan-8-yl)-*N*-phenyl-*N*-(thio-phen-2-ylmethyl)butanamide (36f)

Brown solid, 71 mg, yield 29.1%. Synthesized by the protocol of compound **36a** with **35f** (136 mg, 0.5 mmol) and **18** (115 mg, 0.5 mmol) and purified by flash C18 column chromatography [H₂O (0.1% TFA)/methanol = 50:50–80:20]. ¹H NMR (600 MHz, DMSO-*d*₆) δ 8.62 (s, 1H), 7.37–7.41 (m, 3H), 7.31 (t, 1H, *J* = 7.0 Hz), 7.21 (t, 1H, *J* = 7.8 Hz), 7.15 (d, 1H, *J* = 7.4 Hz), 6.88–6.90 (m, 1H), 6.76–6.80 (m, 4H), 4.97 (s, 2H), 4.55 (s, 2H), 2.57 (br, 4H), 2.34–2.39 (m, 2H), 2.20 (t, 2H, *J* = 6.7 Hz), 2.07 (t, 2H, *J* = 7.4 Hz), 1.63–1.66 (m, 2H), 1.90 (br, 2H), 1.49 (d, 2H, *J* = 13.3 Hz). ¹³C NMR (150 MHz, DMSO-*d*₆) δ 178.01, 173.47, 145.17, 143.78, 141.96, 131.28, 130.97, 130.81, 129.99, 129.68, 128.68, 128.24, 127.82, 119.58, 116.29, 60.46, 60.13, 58.67, 50.94, 48.81, 33.10, 30.25, 24.36. HRMS (ESI): *m/z* calcd. for C₂₈H₃₂N₄O₂S 488.2251, found 489.2323 [M+H]⁺. HPLC purity: 98.9%, *t*_R = 12.334 min.

4.1.17. 4-(4-Oxo-1-phenyl-1,3,8-triazaspiro[4.5]decan-8-yl)-*N*-phenyl-*N*-(thio-phen-3-ylmethyl)butanamide (36g)

Brown solid, 77 mg, yield 31.5%. Synthesized by the protocol of compound **36a** with **35g** (136 mg, 0.5 mmol) and **18** (115 mg, 0.5 mmol) and purified by flash C18 column chromatography [H₂O (0.1% TFA)/methanol = 50:50–80:20]. ¹H NMR (600 MHz, DMSO-*d*₆) δ 8.71 (s, 1H), 7.46–7.47 (m, 1H), 7.38 (t, 2H, *J* = 7.4 Hz), 7.31 (t, 1H, *J* = 6.5 Hz), 7.18–7.24 (m, 5H), 6.98 (d, 1H, *J* = 5.1 Hz), 6.84 (d, 2H, *J* = 7.8 Hz), 6.79 (d, 1H, *J* = 7.4 Hz), 4.84 (s, 2H), 4.58 (s, 2H), 2.83–2.86 (m, 4H), 2.49–2.54 (m, 2H), 2.42 (t, 2H, *J* = 6.9 Hz), 2.12 (t, 2H,



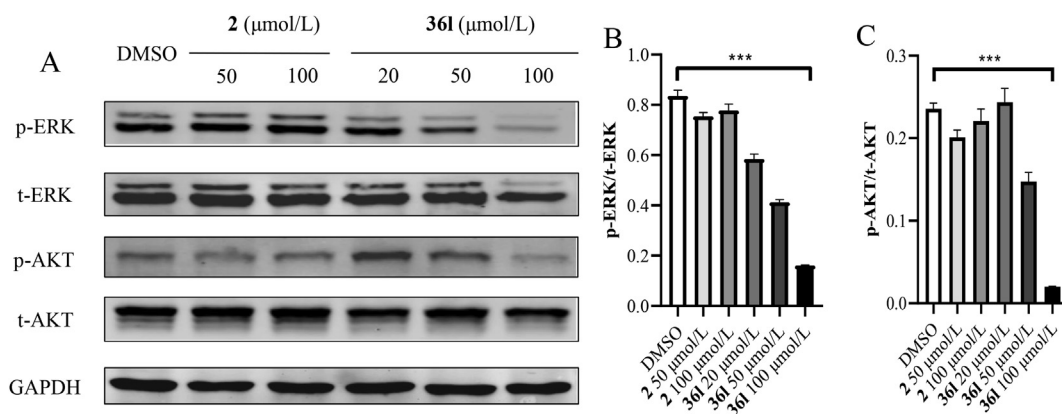


Figure 6 Western blotting analysis of KRAS downstream signal pathways. (A) Phosphorylation levels of t-ERK and t-AKT by stimulated KRAS-dependent Mia PaCa-2 cells with EGF (125 ng/mL, 10 min). From top to bottom: phosphorylated ERK on Thr202 and Tyr204 (p-ERK), total level of ERK (t-ERK), phosphorylated AKT on S473 (p-AKT), total level of AKT (t-AKT), and loading control (GAPDH). (B and C) Gray intensity analysis of the blots in quantification of p-ERK/t-ERK \pm SEM (top) and p-AKT/t-AKT \pm SEM (bottom) was standardized to the EGF-stimulated control (1% DMSO). Data were represented as means \pm SEM, $n = 3$, *** $P < 0.001$.

$J = 6.0$ Hz), 1.72–1.76 (m, 2H), 1.60 (d, 2H, $J = 13.3$ Hz). ^{13}C NMR (150 MHz, DMSO- d_6) δ 176.31, 171.82, 143.69, 142.71, 138.94, 129.88, 129.46, 128.63, 128.18, 126.78, 123.33, 118.32, 114.88, 59.16, 58.33, 56.89, 49.29, 47.95, 31.70, 28.21, 22.15. HRMS (ESI): m/z calcd. for $\text{C}_{28}\text{H}_{32}\text{N}_4\text{O}_2\text{S}$ 488.2251, found 489.2322 $[\text{M}+\text{H}]^+$. HPLC purity: 99.7%, $t_{\text{R}} = 12.682$ min.

4.1.18. 4-(4-Oxo-1-phenyl-1,3,8-triazaspiro[4.5]decan-8-yl)-*N*-phenyl-*N*-(pyridin-2-ylmethyl)butanamide (**36h**)

Brown solid, 63 mg, yield 26.1%. Synthesized by the protocol of compound **36a** with **35h** (134 mg, 0.5 mmol) and **18** (115 mg, 0.5 mmol) and purified by flash C18 column chromatography [H_2O (0.1% TFA)/methanol = 50:50–80:20]. ^1H NMR (600 MHz, DMSO- d_6) δ 8.65 (s, 1H), 7.38 (d, 1H, $J = 2.9$ Hz),

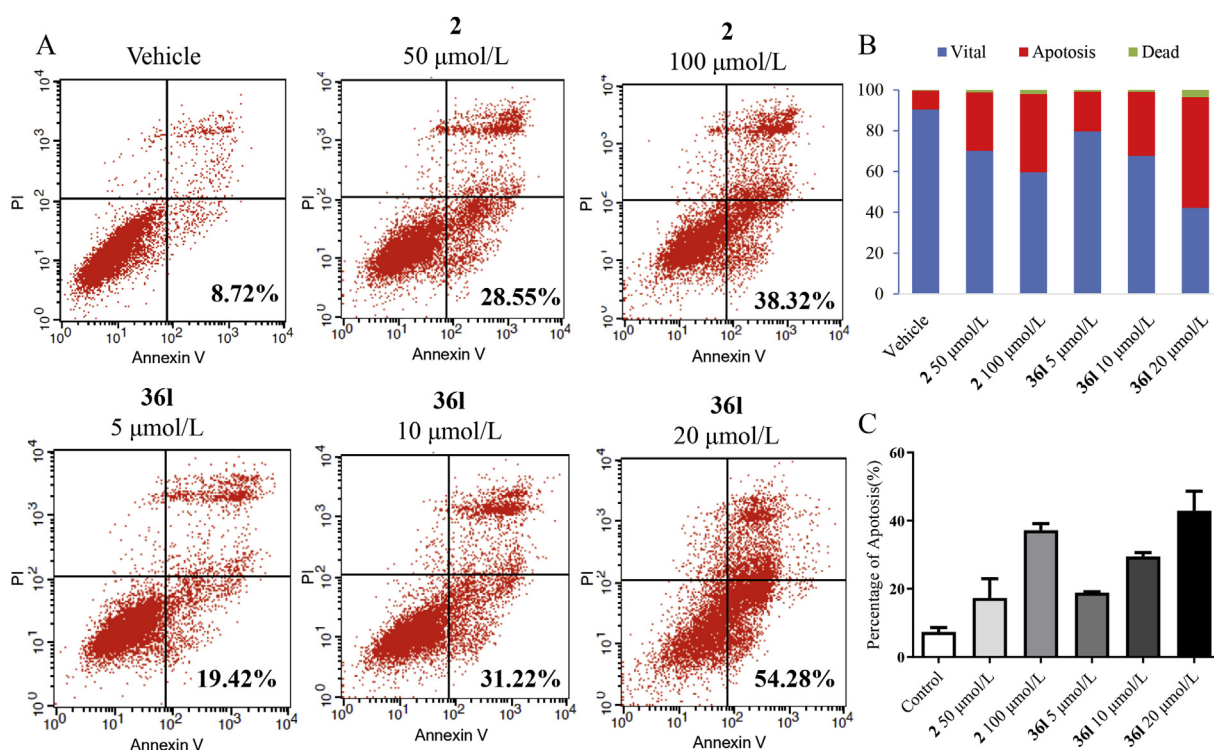


Figure 7 Apoptosis assay staining with Annexin V-FITC/PI in the Mia PaCa-2 cells. (A) Representative scatter plots of samples treated with **2** (50 and 100 $\mu\text{mol/L}$) and compound **361** (5, 10 and 20 $\mu\text{mol/L}$) for 48 h. (B) and (C) Bar charts show quantitative data of apoptosis assay in Mia PaCa-2 cells.

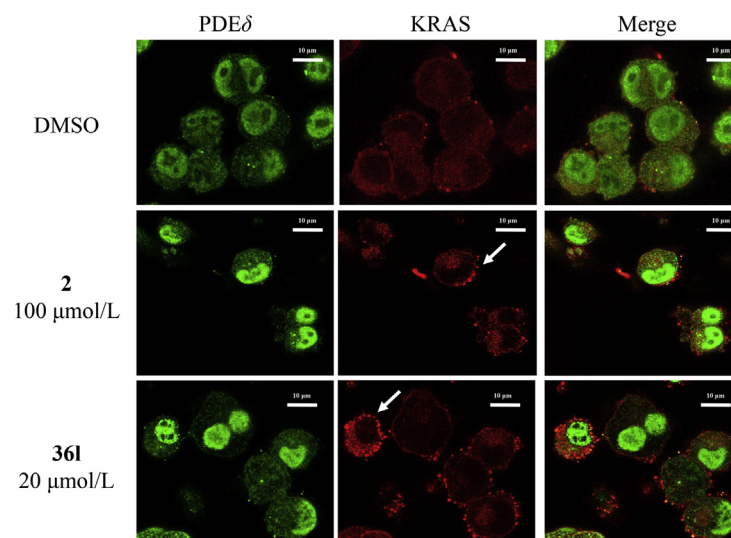


Figure 8 Immunostaining of Mia PaCa-2 cells with anti-PDE δ (green) and anti-KRAS (red) by treated with tested compounds (**2**, 100 $\mu\text{mol/L}$; **361**, 20 $\mu\text{mol/L}$) for 4 h. 1% DMSO was used as the vehicle control. Leica confocal microscope was applied for the image collection. Scale bar: 10 μm .

7.71–7.74 (m, 1H), 7.32–7.36 (m, 5H), 7.27 (t, 1H, $J = 6.9$ Hz), 7.19–7.23 (m, 3H), 6.82 (d, 2H, $J = 7.5$ Hz), 6.79 (t, 1H, $J = 6.9$ Hz), 4.93 (s, 2H), 4.56 (s, 2H), 2.71–2.79 (m, 4H), 2.34–2.46 (m, 4H), 2.18 (br, 2H), 1.71 (br, 2H), 1.56 (d, 2H, $J = 12.9$ Hz). ^{13}C NMR (150 MHz, DMSO- d_6) δ 176.41, 172.30, 157.70, 149.36, 143.73, 143.31, 137.08, 129.88, 129.45, 128.53, 128.09, 122.64, 122.26, 118.27, 114.89, 59.13, 58.50, 57.11, 54.77, 49.47, 31.64, 28.49, 22.54. HRMS (ESI): m/z calcd. for $\text{C}_{29}\text{H}_{32}\text{N}_5\text{O}_2$ 483.2634, found 484.2707 $[\text{M}+\text{H}]^+$. HPLC purity: 97.7%, $t_{\text{R}} = 9.197$ min.

4.1.19. 4-(4-Oxo-1-phenyl-1,3,8-triazaspiro[4.5]decan-8-yl)-N-phenyl-N-(pyridin-4-ylmethyl)butanamide (**36i**)

Brown solid, 68 mg, yield 28.1%. Synthesized by the protocol of compound **36a** with **35i** (134 mg, 0.5 mmol) and **18** (115 mg, 0.5 mmol) and purified by flash C18 column chromatography [H_2O (0.1% TFA)/methanol = 50:50–80:20]. ^1H NMR (600 MHz, DMSO- d_6) δ 8.72 (s, 1H), 8.50 (br, 1H), 7.17–7.38 (m, 10H), 6.82 (d, 2H, $J = 8.7$ Hz), 6.75 (t, 1H, $J = 7.5$ Hz), 4.85 (s, 2H), 4.55 (s, 2H), 2.86–2.90 (m, 4H), 2.50–2.54 (m, 2H), 2.17–2.19 (m, 2H), 1.74–1.76 (m, 2H), 1.60 (d, 2H, $J = 13.7$ Hz). ^{13}C NMR (150 MHz, DMSO- d_6) δ 176.23, 172.45, 150.01, 143.65, 142.69, 130.06, 129.46, 128.48, 128.31, 118.36, 114.91, 59.16, 58.26, 56.78, 49.26, 31.51, 28.09, 21.95. HRMS (ESI): m/z calcd. for $\text{C}_{29}\text{H}_{33}\text{N}_5\text{O}_2$ 483.2634, found 484.2708 $[\text{M}+\text{H}]^+$. HPLC purity: 99.4%, $t_{\text{R}} = 8.833$ min.

4.1.20. 4-(4-Oxo-1-phenyl-1,3,8-triazaspiro[4.5]decan-8-yl)-N-phenyl-N-(quinolin-6-ylmethyl)butanamide (**36j**)

Brown solid, 88 mg, yield 33.0%. Synthesized by the protocol of compound **36a** with **35j** (159 mg, 0.5 mmol) and **18** (115 mg, 0.5 mmol) and purified by flash C18 column chromatography [H_2O (0.1% TFA)/methanol = 50:50–80:20]. ^1H NMR (600 MHz, DMSO- d_6) δ 8.84 (dd, 1H, $J = 1.6, 4.0$ Hz), 8.62 (s, 1H), 8.27 (d, 1H, $J = 8.3$ Hz), 7.70 (s, 1H), 7.96 (d, 1H,

$J = 8.8$ Hz), 7.63 (dd, 1H, $J = 1.9, 8.6$ Hz), 7.46–7.48 (m, 1H), 7.30–7.33 (m, 2H), 7.17–7.25 (m, 5H), 6.73–6.77 (m, 3H), 5.05 (s, 2H), 4.54 (s, 2H), 2.55–2.59 (m, 4H), 2.34–2.39 (m, 2H), 2.22 (t, 2H, $J = 6.4$ Hz), 2.16 (t, 2H, $J = 6.4$ Hz), 1.60–1.72 (m, 2H), 1.49 (d, 2H, $J = 13.6$ Hz). ^{13}C NMR (150 MHz, DMSO- d_6) δ 176.64, 172.60, 150.75, 147.50, 143.80, 142.73, 136.57, 136.24, 130.15, 129.91, 129.55, 129.41, 128.67, 128.16, 128.07, 127.00, 122.05, 118.22, 114.95, 59.09, 58.78, 57.40, 52.31, 49.60, 31.85, 28.91, 23.07. HRMS (ESI): m/z calcd. for $\text{C}_{33}\text{H}_{35}\text{N}_5\text{O}_2$ 533.2791, found 534.2875 $[\text{M}+\text{H}]^+$. HPLC purity: 98.9%, $t_{\text{R}} = 10.733$ min.

4.1.21. 4-(4-Oxo-1-phenyl-1,3,8-triazaspiro[4.5]decan-8-yl)-N-phenyl-N-(quinolin-3-ylmethyl)butanamide (**36k**)

Brown solid, 70 mg, yield 26.2%. Synthesized by the protocol of compound **36a** with **35k** (159 mg, 0.5 mmol) and **18** (115 mg, 0.5 mmol) and purified by flash C18 column chromatography [H_2O (0.1% TFA)/methanol = 50:50–80:20]. ^1H NMR (600 MHz, DMSO- d_6) δ 8.74 (d, 1H, $J = 1.7$ Hz), 8.67 (s, 1H), 8.10 (s, 1H), 7.98 (d, 1H, $J = 8.7$ Hz), 7.93 (d, 2H, $J = 7.7$ Hz), 7.71–7.74 (m, 1H), 7.57–7.58 (m, 1H), 7.33 (t, 2H, $J = 7.7$ Hz), 7.18–7.31 (m, 5H), 6.75–6.82 (m, 3H), 5.08 (s, 2H), 4.57 (s, 2H), 2.75–2.80 (m, 4H), 2.42–2.46 (m, 4H), 2.17 (t, 2H, $J = 6.3$ Hz), 1.73–1.78 (m, 2H), 1.59 (d, 2H, $J = 13.5$ Hz). ^{13}C NMR (150 MHz, DMSO- d_6) δ 176.36, 172.44, 151.47, 147.26, 143.70, 142.43, 135.02, 131.19, 130.05, 129.76, 129.45, 129.12, 128.76, 128.40, 128.31, 127.83, 127.25, 118.36, 114.99, 59.14, 58.41, 57.00, 50.37, 49.40, 31.73, 28.35, 22.30. HRMS (ESI): m/z calcd. for $\text{C}_{33}\text{H}_{35}\text{N}_5\text{O}_2$ 533.2791, found 534.2876 $[\text{M}+\text{H}]^+$. HPLC purity: 96.8%, $t_{\text{R}} = 11.406$ min.

4.1.22. N-(Cyclohexylmethyl)-4-(4-oxo-1-phenyl-1,3,8-triazaspiro[4.5]decan-8-yl)-N-phenylbutanamide (**36l**)

Pale solid, 85 mg, yield 34.8%. Synthesized by the protocol of compound **36a** with **35l** (136 mg, 0.5 mmol) and **18** (115 mg,

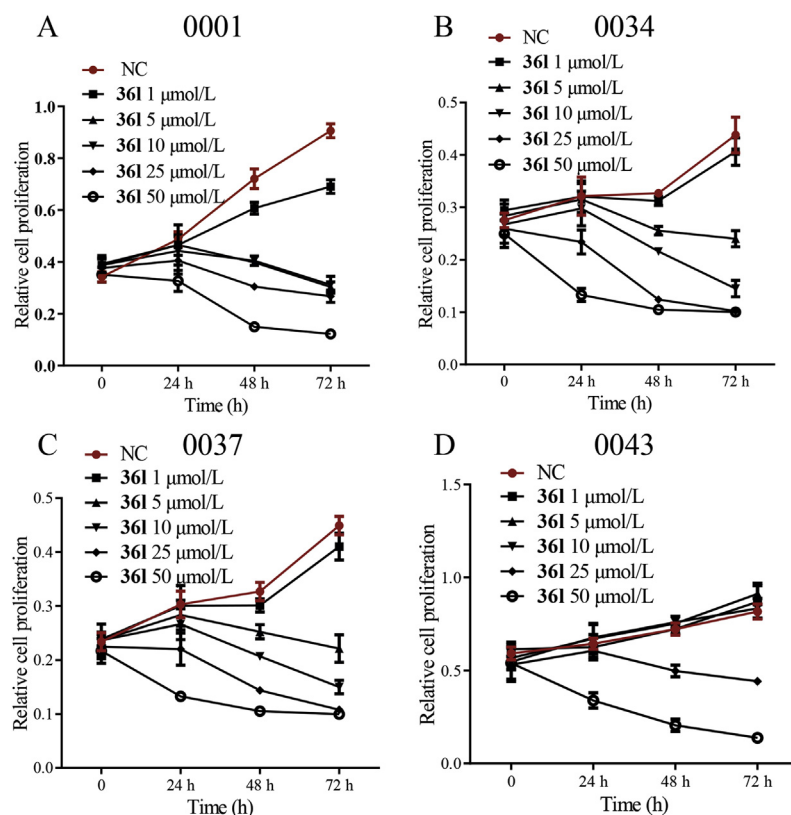


Figure 9 The primary cell lines [0001 ($KRAS^{G12A}$), 0034 ($KRAS^{G12R}$), 0037 ($KRAS^{G12D}$) and 0043 ($KRAS^{G12D}$)] from Ruijin Hospital were treated with **361** at various concentrations for 24, 48 and 72 h, respectively. The percentages of viability were measured by CCK8 method. All the studies with primary cell lines were approved by the Ruijin Hospital Ethics Committee.

0.5 mmol) and purified by flash C18 column chromatography [H_2O (0.1% TFA)/methanol = 50:50–80:20]. 1H NMR (600 MHz, $DMSO-d_6$) δ 8.59 (s, 1H), 7.43 (t, 2H, $J = 7.5$ Hz), 7.29–7.33 (m, 3H), 7.21–7.24 (m, 2H), 6.77–6.79 (m, 3H), 4.93 (s, 2H), 3.51 (d, 2H, $J = 7.5$ Hz), 2.53–2.55 (m, 4H), 2.33–2.39 (m, 2H), 2.17 (t, 2H, $J = 6.2$ Hz), 2.02 (t, 2H, $J = 7.5$ Hz), 1.56–1.64 (m, 7H), 1.50 (d, 2H, $J = 13.0$ Hz), 1.33–1.35 (m, 1H), 1.06–1.11 (m, 3H), 0.87–0.92 (m, 2H). ^{13}C NMR (150 MHz, $DMSO-d_6$) δ 176.23, 171.75, 143.39, 142.96, 129.58, 129.02, 128.24, 127.55, 117.80, 114.49, 58.66, 58.36, 56.98, 54.03, 49.14, 35.73, 31.50, 30.27, 28.45, 26.06, 25.37, 22.62. HRMS (ESI): m/z calcd. for $C_{30}H_{40}N_4O_2$ 488.3151, found 489.3231 $[M+H]^+$. HPLC purity: 99.0%, $t_R = 16.157$ min.

4.1.23. *N*-(Cyclopentylmethyl)-4-(4-oxo-1-phenyl-1,3,8-triazaspiro[4.5]decan-8-yl)-*N*-phenylbutanamide (36m**)**

Pale solid, 86 mg, yield 36.3%. Synthesized by the protocol of compound **36a** with **35m** (130 mg, 0.5 mmol) and **18** (115 mg, 0.5 mmol) and purified by flash C18 column chromatography [H_2O (0.1% TFA)/methanol = 50:50–80:20]. 1H NMR (600 MHz, $DMSO-d_6$) δ 8.70 (s, 1H), 7.49 (t, 2H, $J = 8.1$ Hz), 7.30–7.35 (m, 3H), 7.22 (t, 2H, $J = 7.9$ Hz), 6.77–6.82 (m, 3H), 4.57 (s, 2H), 3.61 (d, 2H, $J = 7.9$ Hz), 2.76 (br, 4H), 2.48–2.50 (m, 2H), 2.35 (t, 2H, $J = 6.0$ Hz), 2.02 (t, 2H, $J = 6.9$ Hz), 1.87–1.92 (m, 1H), 1.66–1.68 (m, 2H), 1.54–1.60 (m, 6H), 1.43–1.45 (m, 2H), 1.15–1.19 (m, 2H). ^{13}C NMR (150 MHz, $DMSO-d_6$) δ 175.90, 171.34, 143.25, 142.47, 129.53, 128.99,

128.32, 127.59, 117.80, 114.38, 58.67, 57.94, 56.59, 52.48, 48.87, 37.75, 31.42, 29.72, 27.86, 24.73, 21.89. HRMS (ESI): m/z calcd. for $C_{29}H_{38}N_4O_2$ 474.2995, found 475.3070 $[M+H]^+$. HPLC purity: 99.2%, $t_R = 15.359$ min.

4.1.24. *N*-(Cyclobutylmethyl)-4-(4-oxo-1-phenyl-1,3,8-triazaspiro[4.5]decan-8-yl)-*N*-phenylbutanamide (36n**)**

White solid, 75 mg, yield 32.6%. Synthesized by the protocol of compound **36a** with **35n** (122 mg, 0.5 mmol) and **18** (115 mg, 0.5 mmol) and purified by flash C18 column chromatography [H_2O (0.1% TFA)/methanol = 50:50–80:20]. 1H NMR (600 MHz, $DMSO-d_6$) δ 8.67 (s, 1H), 7.43 (t, 2H, $J = 7.6$ Hz), 7.34 (t, 2H, $J = 7.3$ Hz), 7.21–7.26 (m, 4H), 6.77–6.81 (m, 3H), 4.56 (s, 2H), 3.70 (d, 1H, $J = 7.6$ Hz), 2.71–2.72 (m, 4H), 2.42–2.47 (m, 2H), 2.29–2.37 (m, 3H), 2.00 (t, 2H, $J = 7.1$ Hz), 1.85–1.91 (m, 2H), 1.73–1.79 (m, 2H), 1.63–1.65 (m, 2H), 1.54–1.61 (m, 4H). ^{13}C NMR (150 MHz, $DMSO-d_6$) δ 175.95, 171.31, 143.26, 142.43, 129.47, 128.98, 128.33, 127.63, 117.79, 114.40, 58.65, 57.99, 56.68, 53.04, 48.94, 33.61, 31.35, 27.99, 25.67, 22.05, 17.80. HRMS (ESI): m/z calcd. for $C_{28}H_{36}N_4O_2$ 460.2838, found 461.2914 $[M+H]^+$. HPLC purity: 99.2%, $t_R = 14.265$ min.

4.1.25. *N*-(Cyclopropylmethyl)-4-(4-oxo-1-phenyl-1,3,8-triazaspiro[4.5]decan-8-yl)-*N*-phenylbutanamide (36o**)**

White solid, 74 mg, yield 33.2%. Synthesized by the protocol of compound **36a** with **35o** (116 mg, 0.5 mmol) and **18** (115 mg, 0.5 mmol) and purified by flash C18 column chromatography

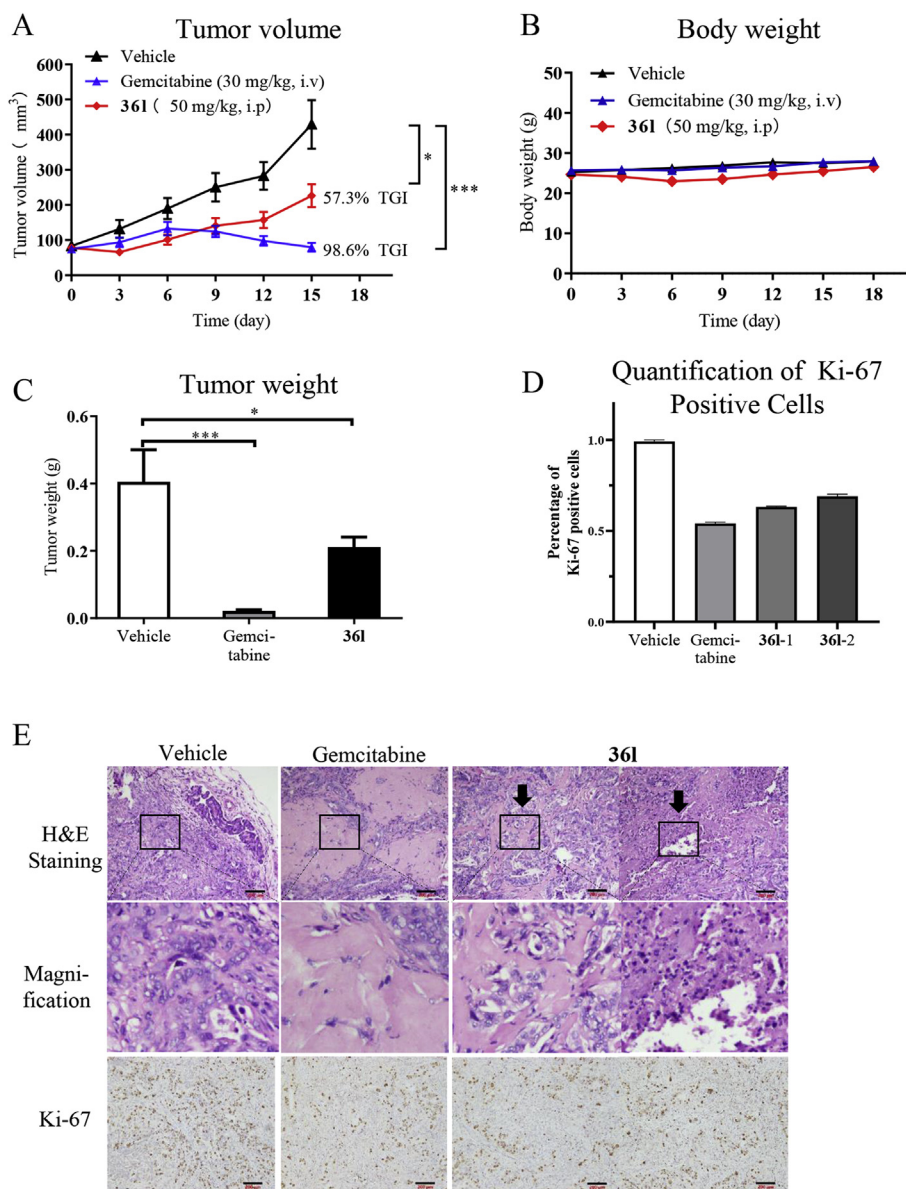


Figure 10 Therapeutic efficacy of compound **361** in the pancreatic tumor PDX model. When the tumor reached about 100 mm³ (set to day 0), the mice were divided into three group randomly. Then, the groups were respectively treated with the compound **361** (50 mg/kg, QD) intraperitoneally, gemcitabine (30 mg/kg, once every 3 days) and saline intravenously until the endpoint. (A) Effect of **361** on tumor volume growth in PDX models. (B) Effect of **361** on body weight in PDX models. (C) Weight of the PDX tumor treated with vehicle, gemcitabine and **361**. (D) Quantification of Ki-67 positive cells³⁸. (E) Representative images of H&E staining and IHC staining for Ki-67 of tumor tissues treated by vehicle, gemcitabine and **361**. Scale bar: 200 μ m. Data were represented as the mean \pm standard deviation, $n = 5$. * $P < 0.05$, ** $P < 0.01$, *** $P < 0.001$.

[H₂O (0.1% TFA)/methanol = 50:50–80:20]. ¹H NMR (600 MHz, DMSO-*d*₆) δ 8.65 (s, 1H), 7.45 (t, 2H, $J = 6.9$ Hz), 7.31–7.37 (m, 3H), 7.21–7.24 (m, 2H), 6.77–6.83 (m, 3H), 4.57 (s, 2H), 3.51 (d, 1H, $J = 6.9$ Hz), 2.69 (br, 4H), 2.45–2.48 (m, 2H), 2.29 (t, 2H, $J = 8.1$ Hz), 2.00 (t, 2H, $J = 6.9$ Hz), 1.64–1.69 (m, 2H), 1.55 (d, 2H, $J = 13.0$ Hz), 0.85–0.91 (m, 1H), 0.36–0.39 (m, 2H), 0.04–0.05 (m, 2H). ¹³C NMR (150 MHz, DMSO-*d*₆) δ 176.48, 171.71, 143.75, 143.17, 129.91, 129.45, 128.99, 128.12, 118.25, 114.89, 59.13, 58.57, 57.26, 52.99, 49.47, 31.90, 28.57, 22.65, 10.34, 3.90. HRMS (ESI): m/z calcd. for

C₂₇H₃₄N₄O₂ 446.2682, found 447.2757 [M+H]⁺. HPLC purity: 97.2%, $t_R = 12.547$ min.

4.2. Fluorescence anisotropy assay

The assay was carried out using our established protocol previously²⁶. In Brief, 80 nmol/L PDE δ protein and 25 nmol/L Atorvastatin-FITC probe in PBS buffer were mix in the plate (Corning 3650). The compounds with various concentrations were added to each well. PBS buffer was supplied until the volume

reached 200 μ L. The plate was incubated at 30 °C for 10 h. The fluorescence anisotropy and fluorescence intensity were detected by Biotek Synergy H2 with 485 nm excitation and 528 nm emission. The results were calculated by Mathematic 9.0 (Wolfram Research).

4.3. Molecular docking

The crystal complex 5X74²⁶ was chosen for the docking study. Firstly, the reliability of the docking method was established with the following procedure: 1) the protocol of protein preparation was according to previous works. The water molecules were removed, hydrogen atoms were complemented and energy minimized with OPLS2005 to the RMSD reaching 0.30 Å; 2) the program LigPrep was used for ligand preparation with OPLS2005 force-field. Other settings follow the default parameters. 20 low energy ring conformations were generated for each ligand; 3) the protein grid was generated by Receptor Grid Generation using H-bond constraints with Agr61, Glu78, Glu88 and Try149. Extra Precision (XP) and H-bond constraints were applied in the docking study. The figures were generated using PyMol academic version (<http://pymol.sourceforge.net/>).

4.4. Determination of the solubility of compounds in water

The solubility assay was conducted according to the literature⁴⁰. In brief, 5 mg compound was dissolved in 1 mL PBS (pH = 7.4) for 24 h in 37 °C. Then the suspension was filtered to afford the saturated solution. Standards in acetonitrile (0.2 mL) with concentration at 1, 0.5, 0.25, 0.125, and 0.0625 mg/mL and saturated solution were added into a quartz 96-well plate. Acetonitrile and PBS solution was added as blank respectively. UV absorbance value at 254 nm was determined with Biotek Synergy H2. The solubility was calculated using the absorbance value and concentration of standards according to Lambert–Beer law.

4.5. Cell culture

Mia PaCa-2 cells were cultured in DMEM (Hyclone) containing 10% fetal bovine serum (Gibco), 2.5% horse serum (Biosharp), 100 U/mL penicillin and 100 μ g/mL streptomycin (Gibco). The primary cell lines were cultured in 1640 (Hyclone) containing 10% fetal bovine serum (Gibco), 100 U/mL penicillin and 100 μ g/mL streptomycin (Gibco). Cells were maintained in a humidified incubator with 95% air/5% CO₂ at 37 °C.

4.6. In vitro antiproliferative assay

Mia PaCa-2 cell line and primary cell lines (0001, 0034, 0037 and 0043) were chosen to determine the inhibitory activity towards pancreatic cancer. The density was 5000 per well in 96-well plates. After cultured for 24 h, each compound was added to triplicate wells at different concentrations and 0.5% DMSO for control. After 72 h of incubation, the medium was removed and 10% CCK8 in DMEM was added to each well following incubating further for the suitable time at 37 °C. The absorbance (OD) at 450 nm was quantitated with Biotek Synergy H2. Wells with no cells and drugs were used as blanks. The concentration inhibited cell growth by 50% (IC₅₀) was calculated by GraphPad Prism 5.0.

4.7. Cell apoptosis assay

Mia PaCa-2 cells were seeded at a density of 3×10^5 cells per well in 6-well plates. After 24 h, the cells were treated with compounds of different concentrations for the proper time. Cells were collected and treated with Annexin V-FITC and PI according to the manufacture's protocol. The stained cells were analyzed by a flow cytometer (BD Accuri C6).

4.8. Western blotting

Mia PaCa-2 cells were seeded at a density of 6×10^5 cells per well in 6-well plates. Then cells were starved and treated with EGF followed by compounds for 2 h as the procedure reported. Then, the protein was extracted, denatured and run on SDS-PAGE gels. Each sample was loaded with 30 μ g total protein. The gels were electroblotted onto polyvinylidene fluoride membrane (0.22 μ m) and blocked for 2 h at room temperature. The primary antibodies used for western blotting were: p44/42 MAPK (ERK1/2) (Cell Signaling Technology # 9107, 1:1000), anti-Phospho AKT (Cell Signaling Technology # 4060, 1:800), anti-AKT1 (Cell Signaling Technology, 1:1000), GAPDH (Abcam, 1:1000), Phospho p44/42 MAPK (ERK1/2) (Thr202/Tyr204) (Cell Signaling Technology # 4370, 1:1000). And secondary FITC-labeled antibodies including goat anti rabbit IgG (Abcam, 1:5000) and goat anti mouse IgG (Abcam, 1:8000) were applied. The blots were scanned on the LI-COR Odyssey imaging system. The gray values of the bands were applied for quantification of the protein level while the control group as the standard.

4.9. CETSA^{41,42}

Prepared the cell in 4 separate 10 cm flasks. Complete medium containing the different concentrations of compounds were added, and the control group containing 1% DMSO. Then cultured the cells for another 2 h. Harvested and re-suspended the cells with 1 mL PBS buffer with protease inhibitors, then divided into 10 tubes. Heated the tubes successively at different temperatures for 3 min, followed by incubation at room temperature for 3 min. Snap-freeze the tube in liquid nitrogen for 3 circles. The cell lysates were reserved on ice after the third snap-freeze. Centrifuge the tubes at 4 °C, 12,000 rpm, 15 min. The supernatant was kept and the loading buffer was added. Then heated the mixture at 70 °C for 10 min. Western blotting experiments and gray-scale statistics were conducted to quantify the protein.

4.10. Co-IP^{43,44}

Six dishes of Mia PaCa-2 cells were prepared. Renewed the medium with 20 μ mol/L compound **361** and 1% DMSO to every 3 dishes respectively and incubated for another 2 h. Harvested and combined the cells, then added 500 μ L of IP lysate (Beyotime, containing 1% protease inhibitor) and lysed the cells on ice for 30 min. The prepared Protein A/G beads (Santa Cruz) were added into the cell lysates. Shacked the tubes at 4 °C for 1 h followed by a centrifuge at 4 °C, 12,000 rpm, 15 min. Quantify the supernatant by the BCA method and adjust the total protein concentration to 5 μ g/mL. Respectively added KRAS primary antibody (Abcam #ab275876) and IgG (Abcam #ab125938) antibody to 100 μ L the above lysates followed by rotating at 4 °C for 1 h. Add the Protein

A/G beads 20 μ L respectively into the supernatant above, and rotated on the shaker overnight. Centrifuged and collected the precipitate followed by washed it with 500 μ L PBS buffer 3 times. Centrifuged and collected the precipitate followed by denaturation in $2 \times$ loading buffer 60 μ L at 95 $^{\circ}$ C for 10 min. Western blotting experiments and gray-scale statistics were conducted to quantify the KRAS and PDE δ protein.

4.11. Immunostaining

After 24 h, the cells were incubated with either 1% DMSO or compounds for 2 h, and then treated as following steps: 1) fixated with 4% paraformaldehyde for 10 min, 2) permeabilized with PBS/0.1% Triton-X for 10 min, 3) blocked with donkey serum blocking buffer [10% donkey serum (Solarbio) in PBS] at a period of 60 min, washed the cells with PBS three times between each steps. The anti-Pan-RAS mouse monoclonal antibody (Calbiochem # OP40-100UG; 1:40) and anti-PDE δ antibody (Genetax # GTX109240, 1:500) were mixed and incubated in blocking buffer overnight at 4 $^{\circ}$ C. Afterwards, the cells were washed with PBS three times. The secondary antibody, Dylight 649 nm goat anti-Mouse antibody (Abbkine; 1:1000) and Alexa 488 nm goat anti-rabbit antibody (abcam #ab150077, 1:1000) was incubated for another 2 h. The cells were washed three times with PBST, and the images were collected by confocal microscopy (Leica TCS SP5 equipped with Argon-Heli-umNenon laser).

4.12. Pharmacokinetic study of compound **361** in vivo

The animal use and care protocols and the experimental procedures were approved by the Committee on Ethics of Biomedicine, Second Military Medical University (Shanghai, China). The compound **361** were chosen for pharmacokinetic study with male ICR mice. The compounds were dissolved in saline containing 1% DMSO and 0.05% CMC-Na and administered intraperitoneally at a dose of 100 mg/kg. Blood samples about 0.05 mL were collected at 1, 2, 4, and 8 h in micro-tubes containing 0.1% heparin. The plasma were afforded by centrifuging the blood samples for 10 min at 4000 rpm, which were further precipitated protein with methanol, centrifuged for 5 min at 12,000 rpm. The supernatant was kept and detected by HPLC. HPLC condition: water (0.1 TFA)/methanol = 40:60–0:100 (15 min), flow rate = 0.6 mL/min. Peak areas of each sample were detected and converted to concentration according to the standard curve. The bioavailability was calculated by GraphPad Prism 5.0.

4.13. Study of in vivo efficacy in PDX mouse model

The PDX model was constructed as the literature⁴⁵. All the studies with mice were approved by the Ruijin Hospital Ethics Committee. In brief, the nude female mice were implanted with passaged PDXs tumors using a trocar. When the tumor reached 100 mm³, the mice were divided into three group randomly. The mice were respectively treated with the compound gemcitabine (30 mg/kg, once every 3 days), saline intravenously and **361** (50 mg/kg, QD) intraperitoneally until the endpoint. The body weight were evaluated. The tumor size was calculated using formula ($L \times W^2$) \times ($\pi/6$), where L is the long axis and W is the width axis. Tumor size and body weight were recorded every 3 days over the

course of study. Mice were sacrificed on Day 14 and all tumors were harvested and analyzed.

4.14. H&E staining and immunochemical staining

All tumor samples were fixed in 10% formaldehyde overnight, then dehydrated in graded concentrations of ethanol. For hematoxylin and eosin (H&E) staining, slides were stained with Mayer's hematoxylin for 2 min, blued in 0.1% sodium bicarbonate for 1 min, washed in water and counterstained with Eosin Y solution for 1 min. For immunohistochemistry, sections were fixed onto poly-L-lysine coated slides. The slides were incubated with rabbit anti-Ki67 antibody (1:500, GB111141, Servicebio, China) in a humid incubator at 4 $^{\circ}$ C overnight. The secondary antibody system (PV9000, Golden Bridge International, Beijing, China) was followed according to the manufacturer's instructions. A positive staining result was recorded when the nucleus of cells was stained yellow or brown. Per slide were randomly chosen to measure the proportion of immunopositive cells. Quantification of Ki-67 positive drug was calculated by ImageJ 1.51.

4.15. Statistical analysis

The Student's t -test and one-way analysis of variance were used for comparison among all different groups represented with the mean values \pm standard errors. A probability of 0.05 or less ($*P < 0.05$, $**P < 0.01$, and $***P < 0.001$) was considered statistically significant.

Acknowledgments

This work was supported by the National Key R&D Program of China (Grant No. 2020YFA0509100), the National Natural Science Foundation of China (Grants 21738002, 82030105, 81725020 and 81903436).

Author contributions

Long Chen synthesized the target compounds and completed most biological and cell-based assays. Jing Zhang and Xinjing Wang constructed the (PDX) models and completed the *in vivo* anti-tumor assays. Yu Li and Lu Zhou participated in research design and conducted experiments. Xiongxiong Lu, Guoqiang Dong and Chunquan Sheng proposed the project, performed data analysis and contributed to the writing—review&editing of the manuscript. All authors have given approval to the final version of the manuscript.

Conflicts of interest

The authors have no conflicts of interest to declare.

Appendix A. Supporting information

Supporting information to this article can be found online at <https://doi.org/10.1016/j.apsb.2021.07.009>.

References

1. Kamerkar S, LeBleu VS, Sugimoto H, Yang S, Ruivo CF, Melo SA, et al. Exosomes facilitate therapeutic targeting of oncogenic KRAS in pancreatic cancer. *Nature* 2017;**546**:498–503.
2. Zhu Z, Xiao S, Hao H, Hou Q, Fu X. Kirsten rat sarcoma viral oncogene homologue (kras) mutations in the occurrence and treatment of pancreatic cancer. *Curr Top Med Chem* 2019;**19**:2176–86.
3. Gillson J, Ramaswamy Y, Singh G, Gorfe AA, Pavlakis N, Samra J, et al. Small molecule KRAS inhibitors: the future for targeted pancreatic cancer therapy?. *Cancers (Basel)* 2020;**12**:1341–9.
4. Bryant KL, Mancias JD, Kimmelman AC, Der CJ. KRAS: feeding pancreatic cancer proliferation. *Trends Biochem Sci* 2014;**39**:91–100.
5. Nagasaka M, Li Y, Sukari A, Ou SI, Al-Hallak MN, Azmi AS. KRAS G12C game of thrones, which direct KRAS inhibitor will claim the iron throne?. *Cancer Treat Rev* 2020;**84**:101974.
6. Misale S, Fothergill JP, Cortez E, Li C, Bilton S, Timonina D, et al. KRAS G12C NSCLC models are sensitive to direct targeting of KRAS in combination with PI3K inhibition. *Clin Cancer Res* 2019;**25**:796–807.
7. Nollmann FI, Ruess DA. Targeting mutant KRAS in pancreatic cancer: futile or promising?. *Biomedicines* 2020;**8**:281–94.
8. Seton-Rogers S. KRAS-G12C in the crosshairs. *Nat Rev Cancer* 2020;**20**:3.
9. Canon J, Rex K, Saiki AY, Mohr C, Cooke K, Bagal D, et al. The clinical KRAS(G12C) inhibitor AMG 510 drives anti-tumour immunity. *Nature* 2019;**575**:217–23.
10. Hata AN, Shaw AT. Resistance looms for KRAS(G12C) inhibitors. *Nat Med* 2020;**26**:169–70.
11. Veluswamy R, Mack PC, Houldsworth J, Elkhoully E, Hirsch FR. KRAS G12C-mutant non-small cell lung cancer: biology, developmental therapeutics, and molecular testing. *J Mol Diagn* 2021;**23**:507–20.
12. Kim D, Xue JY, Lito P. Targeting KRAS(G12C): from inhibitory mechanism to modulation of antitumor effects in patients. *Cell* 2020;**183**:850–9.
13. Grapsa D, Syrigos K. Direct KRAS inhibition: progress, challenges, and a glimpse into the future. *Expert Rev Anticancer Ther* 2020;**20**:437–40.
14. Khan I, Rhett JM, O'Bryan JP. Therapeutic targeting of RAS: new hope for drugging the "undruggable". *Biochim Biophys Acta Mol Cell Res* 2020;**1867**:118570–85.
15. Jones GD, Caso R, Tan KS, Mastrogiacomo B, Sanchez-Vega F, Liu Y, et al. KRAS (G12C) mutation is associated with increased risk of recurrence in surgically resected lung adenocarcinoma. *Clin Cancer Res* 2021;**27**:2604–12.
16. Suladze S, Ismail S, Winter R. Thermodynamic, dynamic and solvational properties of PDE δ binding to farnesylated cysteine: a model study for uncovering the molecular mechanism of PDE δ interaction with prenylated proteins. *J Phys Chem B* 2014;**118**:966–75.
17. Zimmermann G, Papke B, Ismail S, Vartak N, Chandra A, Hoffmann M, et al. Small molecule inhibition of the KRAS–PDE δ interaction impairs oncogenic KRAS signalling. *Nature* 2013;**497**:638–42.
18. Chandra A, Grecco HE, Pisupati V, Perera D, Cassidy L, Skoulidis F, et al. The GDI-like solubilizing factor PDE δ sustains the spatial organization and signalling of Ras family proteins. *Nat Cell Biol* 2011;**14**:148–58.
19. Martin-Gago P, Fansa EK, Wittinghofer A, Waldmann H. Structure-based development of PDE δ inhibitors. *Biol Chem* 2017;**398**:535–45.
20. Papke B, Murarka S, Vogel HA, Martin-Gago P, Kovacevic M, Truxius DC, et al. Identification of pyrazolopyridazinones as PDE δ inhibitors. *Nat Commun* 2016;**7**:11360–8.
21. Murarka S, Martin-Gago P, Schultz-Fademrecht C, Al Saabi A, Baumann M, Fansa EK, et al. Development of pyridazinone chemotypes targeting the pde δ prenyl binding site. *Chemistry (Easton)* 2017;**23**:6083–93.
22. Martin-Gago P, Fansa EK, Klein CH, Murarka S, Janning P, Schurmann M, et al. A PDE δ -KRAS inhibitor chemotype with up to seven H-bonds and picomolar affinity that prevents efficient inhibitor release by Arl2. *Angew Chem Int Ed Engl* 2017;**56**:2423–8.
23. Chen D, Chen Y, Lian F, Chen L, Li Y, Cao D, et al. Fragment-based drug discovery of triazole inhibitors to block PDE δ -RAS protein–protein interaction. *Eur J Med Chem* 2019;**163**:597–609.
24. Leung EL, Luo LX, Li Y, Liu ZQ, Li LL, Shi DF, et al. Identification of a new inhibitor of KRAS–PDE δ interaction targeting KRAS mutant non-small cell lung cancer. *Int J Cancer* 2019;**145**:1334–45.
25. Siddiqui FA, Alam C, Rosenqvist P, Ora M, Sabt A, Manoharan GB, et al. PDE δ inhibitors with a new design principle selectively block K-Ras activity. *ACS Omega* 2020;**5**:832–42.
26. Jiang Y, Zhuang C, Chen L, Lu J, Dong G, Miao Z, et al. Structural biology-inspired discovery of novel KRAS-PDE δ inhibitors. *J Med Chem* 2017;**60**:9400–6.
27. Chen L, Zhuang C, Lu J, Jiang Y, Sheng C. Discovery of novel KRAS-PDE δ inhibitors by fragment-based drug design. *J Med Chem* 2018;**61**:2604–10.
28. Dong G, Chen L, Zhang J, Liu T, Du L, Sheng C, et al. Discovery of turn-on fluorescent probes for detecting PDE δ protein in living cells and tumor slices. *Anal Chem* 2020;**92**:9516–22.
29. Cheng J, Li Y, Wang X, Dong G, Sheng C. Discovery of novel PDE δ degraders for the treatment of KRAS mutant colorectal cancer. *J Med Chem* 2020;**63**:7892–905.
30. Wang S, Zhang Y, Dong G, Wu S, Zhu S, Miao Z, et al. Asymmetric synthesis of chiral dihydrothiopyrans via an organocatalytic enantioselective formal thio [3 + 3] cycloaddition reaction with binucleophilic diketone thioethers. *Org Lett* 2013;**15**:5570–3.
31. Wang S, Jiang Y, Wu S, Dong G, Miao Z, Zhang W, et al. Meeting organocatalysis with drug discovery: asymmetric synthesis of 3,3'-spirooxindoles fused with tetrahydrothiopyrans as novel P53-MDM2 inhibitors. *Org Lett* 2016;**18**:1028–31.
32. Wu S, Li Y, Xu G, Chen S, Zhang Y, Liu N, et al. Novel spiro-pyrazolone antitumor scaffold with potent activity: design, synthesis and structure–activity relationship. *Eur J Med Chem* 2016;**115**:141–7.
33. Wang S, Chen S, Guo Z, He S, Zhang F, Liu X, et al. Synthesis of spiro-tetrahydrothiopyran-oxindoles by Michael-aldol cascade reactions: discovery of potential P53-MDM2 inhibitors with good antitumor activity. *Org Biomol Chem* 2018;**16**:625–34.
34. Chambers M, Delport A, Hewer R. The use of the cellular thermal shift assay for the detection of intracellular beta-site amyloid precursor protein cleaving enzyme-1 ligand binding. *Mol Biol Rep* 2021;**48**:2957–62.
35. Chernobrovkin AL, Cazares-Korner C, Friman T, Caballero IM, Amadio D, Martinez Molina D. A tale of two tails: efficient profiling of protein degraders by specific functional and target engagement readouts. *SLAS Discov* 2021;**26**:534–46.
36. Husain A, Begum NA, Kobayashi M, Honjo T. Native co-immunoprecipitation assay to identify interacting partners of chromatin-associated proteins in mammalian cells. *Bio Protoc* 2020;**10**:e3837.
37. Zhang J, He S. Co-immunoprecipitation assay for blue light-dependent protein interactions in plants. *Methods Mol Biol* 2021;**2297**:141–6.
38. Del Rosario Taco Sanchez M, Soler-Monso T, Petit A, Azcarate J, Lasheras A, Artal C, et al. Digital quantification of KI-67 in breast cancer. *Virchows Arch* 2019;**474**:169–76.
39. Morciano G, Preti D, Pedriali G, Aquila G, Missiroli S, Fantinati A, et al. Discovery of novel 1,3,8-triazaspiro[4.5]decane derivatives that

- target the c subunit of f1/fo-adenosine triphosphate (ATP) synthase for the treatment of reperfusion damage in myocardial infarction. *J Med Chem* 2018;**61**:7131–43.
40. Roy D, Ducher F, Laumain A, Legendre JY. Determination of the aqueous solubility of drugs using a convenient 96-well plate-based assay. *Drug Dev Ind Pharm* 2001;**27**:107–9.
 41. Jafari R, Almqvist H, Axelsson H, Ignatushchenko M, Lundback T, Nordlund P, et al. The cellular thermal shift assay for evaluating drug target interactions in cells. *Nat Protoc* 2014;**9**: 2100–22.
 42. Seashore-Ludlow B, Axelsson H, Lundback T. Perspective on CETSA literature: toward more quantitative data interpretation. *SLAS Discov* 2020;**25**:118–26.
 43. Tang Z, Takahashi Y. Analysis of protein–protein interaction by co-ip in human cells. *Methods Mol Biol* 2018;**1794**:289–96.
 44. Lin JS, Lai EM. Protein–protein interactions: co-immunoprecipitation. *Methods Mol Biol* 2017;**1615**:211–9.
 45. Wen CL, Huang K, Jiang LL, Lu XX, Dai YT, Shi MM, et al. An allosteric PGAM1 inhibitor effectively suppresses pancreatic ductal adenocarcinoma. *Proc Natl Acad Sci U S A* 2019;**116**:23264–73.